

Electronic Thesis and Dissertation Repository

---

4-19-2023 2:30 PM

## Identifying Sources Of Error In Computer Navigated Total Knee Arthroplasties Using A Metric On SE(3) and Sensitivity Analyses

Nicole E. Martensson, *Western University*

Supervisor: Mclsaac, Kenneth, *The University of Western Ontario*

A thesis submitted in partial fulfillment of the requirements for the Master of Engineering Science degree in Electrical and Computer Engineering

© Nicole E. Martensson 2023

Follow this and additional works at: <https://ir.lib.uwo.ca/etd>



Part of the [Other Electrical and Computer Engineering Commons](#)

---

### Recommended Citation

Martensson, Nicole E., "Identifying Sources Of Error In Computer Navigated Total Knee Arthroplasties Using A Metric On SE(3) and Sensitivity Analyses" (2023). *Electronic Thesis and Dissertation Repository*. 9258.

<https://ir.lib.uwo.ca/etd/9258>

This Dissertation/Thesis is brought to you for free and open access by Scholarship@Western. It has been accepted for inclusion in Electronic Thesis and Dissertation Repository by an authorized administrator of Scholarship@Western. For more information, please contact [wlsadmin@uwo.ca](mailto:wlsadmin@uwo.ca).

## Abstract

Throughout the procedure of a computer-navigated total knee arthroplasty (TKA), there are many opportunities for sources of error to be introduced. Identifying these errors can improve surgical outcomes. There is also a lack of accessible methods in available literature for clinicians to perform research in this area using engineering analysis techniques. This thesis aims to provide a greater understanding of the sources of error that can occur pre-bone cut. Possible sources of error include the bony landmark selections and the placement of the cut guide. Using artificial bone models and a 3D point capture system concurrently with a computer-navigation system, the data points collected during the procedure are mimicked. It was found that variability of point selection varied between landmarks with some being more precise than others. Bone reference frames can be calculated using these landmark points. By painting the surface of the saw blade, the cut plane values, and a reference frame for the cuts, can also be estimated. These frames are easily represented with homogeneous transformation matrices. One method of comparing transformation matrices is with a metric on  $SE(3)$ , simplified in this thesis to be the Frobenius norm. It was found that bone reference frames with the highest metric were the ones with the highest error in femur or tibia center points. It was also found that there was no clear correlation between the bone reference frame error and cut plane error, implying that other sources must be taken into account. Sensitivity analyses were performed to observe the outcome error of the bone reference frame and cut plane in regards to error in the landmark selection. The results from this support other results in this thesis: that landmark points used for the origin of the reference frames have the greatest effect on the system output. The methods in this thesis can easily be applied to other computer-navigated systems for analysis.

**Keywords:** Computer Navigated Surgery, Total Knee Arthroplasty, Sensitivity Analysis

## Lay Summary

The use of technology to assist orthopedic procedures such as computer-navigated total knee arthroplasty (TKA) has shown to improve accuracy of the implant placement, leading to higher patient satisfaction. Computer-navigated procedures are when a camera and trackers are used to create a digital model of the bone in order to assist surgeons in the placement of their cuts. However, longer operation times and a steeper learning curve for surgeons remains a concern for these procedures. As well, there are various aspects of the procedure where error can occur. Identifying and explaining these errors can help surgeons be more confident in their decisions during surgery. The main step of computer-navigation is selecting bony landmarks, which the computer then uses to create its digital model of the bone, called a reference frame. To analyze the impact of selecting landmarks incorrectly, a computer-navigated surgery was simulated with another point capture system concurrently on artificial bones. It was found that the same surgeon did not always choose certain landmark points in the same spot every time. The bone reference frames were represented with a homogeneous transformation matrix, which identifies its position and orientation in 3D space. When analyzing the difference between these frames, it was found that certain landmark points had a greater effect on them than others. Also, there are other places where errors can be introduced such as when the surgeon is placing the cut guide manually. Two methods of sensitivity analysis were also performed which analyze how an error in input affects the error in output. It was found that certain landmarks, particularly the center points of the knee, had a much larger effect on the output of the model than others. This work shows that there are multiple sources of error that surgeons must consider, and some sources have a greater affect than others.

Dedicated to: Mia



## Acknowledgements

I would like to thank my supervisor, Dr. Ken McIsaac, for giving me the opportunity to perform this research and for his support and guidance, especially when obstacles were encountered during this work. I would also like to thank Dr. Brent Lanting for his mentorship, for sharing his knowledge, and for providing a direction for this research.

I want to acknowledge Dr. Kellee Stephens who performed several hours of experiments for the data collection of this work and provided valuable information while doing so. Thank you as well to Dr. Ryan Willing who provided use of his equipment, custom software, and lab space for experiments.

Thank you to my research group for always being available to help when questions arose. I would like to thank Delaney Stevens for all her invaluable help and for taking this robotic surgery journey with me. Lastly, I would like to thank my friends and family, especially my parents Peter and Rosanna, for their love and support.

This work was funded in part by scholarships awarded to N. Martensson from the Canada Graduate Scholarship and the Ontario Graduate Scholarship.

# Table of Contents

<b>Abstract</b> .....	i
<b>Lay Summary</b> .....	ii
<b>Acknowledgements</b> .....	iv
<b>Table of Contents</b> .....	v
<b>List of Figures</b> .....	viii
<b>Chapter 1</b> .....	1
<b>Introduction</b> .....	1
1.1 Motivation.....	1
1.2 Tasks and Thesis Contribution.....	3
1.3 Thesis Overview .....	4
<b>Chapter 2</b> .....	5
<b>Background</b> .....	5
2.1 Anatomical Terms and the Knee.....	5
2.1.1 Femoral Landmarks .....	7
2.1.2 Tibial Landmarks .....	9
2.2 Total Knee Arthroplasty .....	10
2.2.1 Cut Decision.....	11
2.3 Computer-navigated TKA .....	12
2.4 Errors in Computer Navigated Systems.....	15
2.5 Reference Frames.....	17
2.5.1 Femoral Reference Frame.....	18
2.5.2 Tibial Reference Frame.....	22

2.6 Homogeneous Transformation Matrices.....	23
2.7 Metric on SE(3).....	25
2.8 Sensitivity Analysis .....	27
2.8.1 Monte Carlo Simulation.....	28
2.8.2 Sensitivity Function using Numerical Differentiation.....	30
<b>Chapter 3</b> .....	<b>32</b>
<b>Methods</b> .....	<b>32</b>
3.1 Physical Data Collection.....	32
3.1.1 Bone Models and Mounting Structure.....	32
3.1.2 Intellijoint KNEE Workflow.....	35
3.1.3 Optotrak Certus.....	38
3.1.4 Data Point Collection.....	39
3.2 Reference Frame and Cut Plane Calculation .....	41
3.2.1 Femoral Reference Frame.....	41
3.2.2 Tibial Reference Frame.....	43
3.2.3 Defining the Cut Planes .....	45
3.3 Transformation Matrices.....	47
3.4 Point Error and Metric Calculation.....	50
3.5 Sensitivity Analysis .....	51
3.5.1 Monte Carlo Simulation.....	51
3.5.2 Numerical Differentiation.....	52
<b>Chapter 4</b> .....	<b>55</b>
<b>Results and Discussion</b> .....	<b>55</b>
4.1 Surgeon Variability.....	55
4.2 Metric on SE(3).....	57

4.2.1	Bone Reference Frames .....	58
4.2.2	Cut Planes .....	60
4.3	Error Cloud .....	65
4.4	Sensitivity Analysis .....	68
4.4.1	Monte Carlo Simulation.....	68
4.4.2	Numerical Differentiation.....	75
<b>Chapter 5</b>	.....	<b>78</b>
<b>Conclusion</b>	.....	<b>78</b>
5.1	Summary .....	78
5.2	Limitations and Future Work.....	79
<b>References</b>	.....	<b>81</b>
<b>Appendix A</b>	.....	<b>93</b>
<b>Appendix B</b>	.....	<b>94</b>



## List of Figures

Figure 2.1: Relevant anatomical terms of the human body .....	5
Figure 2.2: Planes of the human body. ....	6
Figure 2.3: Bones and ligaments of the knee joint.....	7
Figure 2.4: Landmark points of the femur .....	8
Figure 2.5: The three axes that can be determined from landmarks on the distal femur. .	9
Figure 2.6: Landmark points of the tibia. ....	10
Figure 2.7: TKA implants. ....	11
Figure 2.8:Valgus (A), normal (B) and varus (C) leg alignment.....	12
Figure 2.9: Computer-navigated TKA equipment .....	14
Figure 2.10: The femoral bone reference frame from two different views.. ....	20
Figure 2.11: The tibial bone reference frame.....	23
Figure 2.12: An example of a histogram plot produced in Matlab.....	29
Figure 3.1: SolidWorks part model of the acetabular cup mount.....	34
Figure 3.2: Mounting structure for the knee joint with the sawbone mounted inside the acetabular cup model and clamped to the mount.....	35
Figure 3.3: A. Varus/valgus cut on distal femur. B. Flexion cut on distal femur. C. Depth resection on distal femur.....	38
Figure 3.4: Optotrak Certus camera.....	39
Figure 3.5: Infrared emitting trackers (encased in white) that mount onto bone screws and the stylus for the Optotrak Certus .....	39

Figure 3.6: SolidWorks part model of tool used for tracing a line along the probe tracker .....	40
Figure 3.7: Experimental set up for data collection.....	41
Figure 3.8: The femoral coordinate system shown in reference to the pin coordinate system with origin at the femur center.....	43
Figure 3.9: The tibial coordinate system shown in reference to the pin coordinate system with origin at the tibia center .....	44
Figure 3.10: Plot of gathered cloud of cut plane points (green), the mechanical axis of the bone with origin at the femur center (blue) and the intersection point of the cut plane and the mechanical axis (pink) .....	45
Figure 3.11: Plot showing the bone reference frame (in the same colours as used in Figure 3.8) and the reference frame of the cut plane with the normal line to the plane (z-axis) shown in purple and the x and y axes shown in green.....	47
Figure 3.12: Plot showing the collected condyle data points.....	50
Figure 3.13: Cloud of erroneous points used for a landmark, with the true landmark point being at the center in red. ....	52
Figure 3.14: Code workflow for the numerical differentiation method of sensitivity analysis.....	54
Figure 4.1: Plot comparing the metric on SE(3) values between the bone reference frame and the cut plane .....	63
Figure 4.2: Error cloud points for the femur.....	66
Figure 4.3: Error cloud points for the tibia .....	67
Figure 4.4: Combined plot of the femur and tibia density errors.....	68

Figure 4.5: A diagram depicting the concept of angular difference for points at different distances.....	70
Figure 4.6: The results of the Monte Carlo for the femur center.....	71
Figure 4.7: The results of the Monte Carlo for the hip center.. ..	72
Figure 4.8: The results of the Monte Carlo for Whiteside’s line.....	72
Figure 4.9: The plot on the left shows the Monte Carlo results for a disturbance of 1 mm of the femur center in red, Whiteside’s line in blue, and hip center in green. The plot on the right is a zoomed in image so that the hip center points are visible. ....	73
Figure 4.10: Histogram plots of the cut plane error when the femur center is disturbed by A. 1 mm, B. 2 mm, C. 3 mm, and D. 4 mm.....	74

## List of Tables

Table 3.1: Size data for bone models used .....	33
Table 3.2: Cut value goals. ....	37
Table 4.1: Femur landmark error average and sample standard deviation compared to the average point.....	56
Table 4.2: Tibia landmark error average and sample standard deviation compared to the average point.....	56
Table 4.3: Metric on SE(3) values and landmark differences for the sawbone femur .....	58
Table 4.4: Metric on SE(3) values and landmark differences for the sawbone tibia.....	59
Table 4.5: Metric on SE(3) values and cut parameters as reported by the navigation system for the sawbone femur .....	61
Table 4.6: Metric on SE(3) values and cut parameters as reported by the navigation system for the 3D printed femur .....	61
Table 4.7: Metric on SE(3) values and cut parameters as reported by the navigation system for the sawbone tibia.....	62
Table 4.8: Metric on SE(3) values and cut parameters as reported by the navigation system for the 3D printed tibia.....	62
Table 4.9: Results from Monte Carlo simulation of the average error of the bone reference frame for erroneous spheres of increasing size.....	69
Table 4.10: Sensitivity coefficients for the affect of landmarking error for experiment SB-3.....	76
Table 4.11: Various outcomes of the metric on SE(3) values (error in the bone reference frame) with varying inputs for disturbances to the landmark values.....	77

Table B.1 Hip center calculation method comparison.....	94
Table B.2 Femur landmark errors compared to average.....	95
Table B.3 Tibia landmarks compared to average .....	96
Table B.4 Bone reference frame metric values for 3D printed bone .....	97
Table B.5 Lateral and Medial Condyle Errors from Ideal Trial along mechanical axis...	97
Table B.6 Lateral and Medial Plateau Errors from Ideal Trial along mechanical axis ....	98

## List of Acronyms and Variables

**AP** Anterior-Posterior

**FC** Femur Center

**H** Variable used to represent general transformation matrix

**HC** Hip Center

**J** Jacobian Matrix

**LC** Lateral Condyle

**LM** Lateral Malleoli

**LP** Lateral Plateau

**MC** Medial Condyle

**MM** Medial Malleoli

**MP** Medial Plateau

**PCA** Posterior Condylar Axis

**SB** Sawbone

**TC** Tibia Center

**TD** 3D Printed Bone

**TEA** Trans Epicondylar Axis

**TKA** Total Knee Arthroplasty

**WS** Whiteside's Line

$\lambda$  Variable representing disturbance to input of a function

# Chapter 1

## Introduction

### 1.1 Motivation

As Canada's population ages, arthritis will become more prevalent. It is projected that the population of people living with arthritis will increase by 50% to about 9 million people by 2040 [1]. As the health care system struggles to meet demand, it is more important than ever that hospital resources and time are used efficiently.

One treatment for severe arthritis in the knee is a total knee arthroplasty (TKA). This procedure replaces the patient's diseased knee with a synthetic implant, allowing them to restore their range of motion and decrease pain during movement. Advancements have been made over the years to increase accuracy of the procedure. Accuracy refers to the placement of the implant, and this is important because it is theorized that a more correctly placed implant results in a lower probability of the patient needing revision surgery [2] and in a greater probability of the patient having higher satisfaction [3]. Reducing the number of revisions also means more hospital resources would be freed for other purposes.

A popular tool used to improve implant positioning is computer-navigation [4]. This is when the patient's knee is digitized using an optical tracking system by selecting bony landmarks, a cut guide is placed by the surgeon (with information provided from the navigation system), the bone is resected (cut), and the implant placed. Computer-navigation is also the first step in the most recent and major TKA technological advancement which is robotic-assisted surgery. The first aspect (digitization) remains the

same with a manipulator then placing the cutting guide based on the data obtained. However, to ensure the benefits of these systems are fully realized, it is imperative that surgeons be well trained and confident in their understanding of the system.

Two drawbacks often listed for computer navigated TKA (as opposed to conventional TKA) are the increased operating times and steeper learning curve for surgeons [5]. A study found that computer navigated TKA had about a 22 minute longer operation time compared to conventional TKA [6]. A longer operating time can lead to an increased risk of infection. As well, a greater operating time means that hospital resources are occupied for longer. Therefore, even though the procedure is more accurate, that accuracy cannot be outweighed by the decrease in speed or the amount of training it takes for surgeons to learn the system.

It has been reported in literature that there are several sources of error that can occur during computer navigated TKA and that surgeons must be aware of those errors. If they had a greater understanding of why these errors occur and how best to avoid them, it could potentially save time during the surgery as steps do not need to be questioned on their accuracy or reperformed. It will also likely result in a more accurate position of the implant. The error caused by the saw during the bone resection phase has been described in literature [2]. There are errors associated with the landmark and digitization phase of the bone; however, several studies have limitations and there are some gaps in analysis. As well, the errors associated with placement of the cut guide have not been extensively studied. Several methods also take a clinical approach of analyzing the error when an engineering approach could also be beneficial to surgeons in providing a greater understanding of why the computer calculates things the way it does. Therefore, an accessible method for clinicians to perform an engineering analysis is also needed. The work in this thesis aims to benefit orthopedic surgeons and the research community in the following ways:

- Address the gaps in previous research performed on the errors that occur in the pre-bone cutting steps of the procedure.



- Explain why those errors are occurring so that a deeper understanding can be given to clinicians on how to avoid them.
- Provide a workflow for clinicians and researchers alike to continue this analysis in the future.

These goals are especially relevant as technological procedures for TKA grow in popularity at hospitals. For example, the outcomes will have value to the orthopedic group at University Hospital at the University of Western Ontario. They use computer-navigated systems in their operating rooms and are beginning to receive different robotic systems for clinical and research use (systems that rely on computer-navigation as well). Understanding what contributes to inaccuracies of the system can improve patient outcome and allow for resources to be used more efficiently.

## 1.2 Tasks and Thesis Contribution

The pre-resection error of computer-navigated systems is often quantified by the angular difference of the cut guide placement in two planes or the estimated implant placement [7], [8]. However, this does not address the error that could occur with resection depth (i.e., there could be deviation of the cut in rotation and translation from the goal cut). A way to analyze this is with homogeneous transformation matrices since they include both position and orientation. They are also relevant as robotic TKA becomes more popular as they are a fundamental concept in robotics. Analyzing the difference between transformation matrices is difficult though since one matrix includes different units (angular and length). A concept referred to as a metric on  $SE(3)$  can address this concern and provide a means for analyzing error. In this context, a metric is used to describe the distance between two transformation matrices, which can be used to analyze experimental results. The work in this thesis aims to use that concept to provide the benefits listed above. Also, experimental and simulated data are used separately and in combination to see if the same conclusions about sources of error can be reached.

### 1.3 Thesis Overview

This thesis includes the following sections: Chapter 2 discusses the background on concepts related to total knee arthroplasty and the engineering methods and analysis used in this work. It also provides a literature review on other studies that have analyzed errors in computer navigated TKA. Chapter 3 describes the methods used in this thesis including the equipment used, the experimental procedure, and the code used to perform the calculations. Chapter 4 provides the results of the experiments and discusses their implications. Chapter 5 concludes the work with a summary and suggestions for future work. Appendix A provides the reference frame code for the sensitivity function and Appendix B provides supplementary tables of results.

# Chapter 2

## Background

### 2.1 Anatomical Terms and the Knee

Anatomical terminology is used when discussing clinical procedures such as total knee replacements. The relevant terms are discussed here. Proximal means towards the origin of a part, distal means away (for example, the foot is distal to the knee). The distal end of the femur and the proximal end of the tibia are what comprises the knee joint. Anterior refers to the front of the body and posterior refers to the back. Medial means it is towards the body's midline and lateral means away from it [9]. These terms are shown in Figure 2.1.

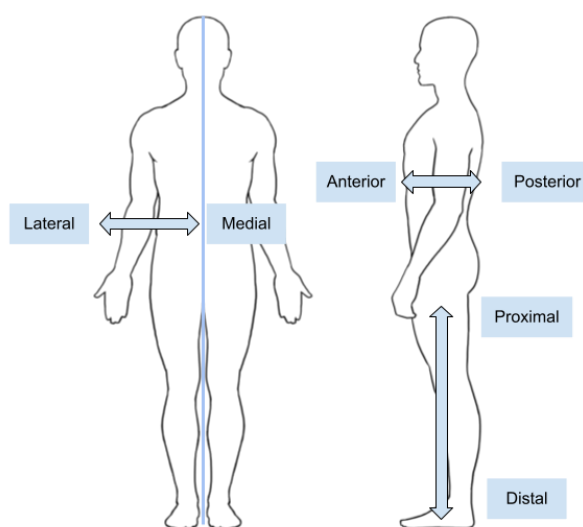


**Figure 2.1: Relevant anatomical terms of the human body**

The body is also divided into 3 planes. The coronal plane separates the anterior side of the body from the posterior, sagittal separates the medial and lateral sides, and transverse (axial) separates superior (towards the head, upper area of body) from inferior (towards the feet, lower area of body) [9]. These are shown in Figure 2.2.

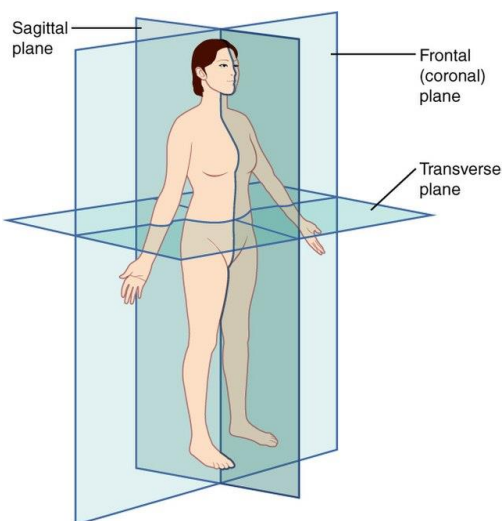


**Figure 2.2: Planes of the human body [10]. Reproduced under the Creative Commons Attribution 4.0 License.**

The knee is comprised of four bones: the femur (thigh bone), the tibia (shin bone), fibula (parallel to the tibia) and the patella (kneecap) [11]. The joint of the knee is comprised of the distal end of the femur and the proximal end of the tibia. The patella also contributes to the function of the knee joint but is not considered during the initial cut performed during total knee arthroplasty (the focus of this thesis) and so it is not discussed. Four ligaments help hold the knee together: the anterior cruciate ligament (ACL), posterior cruciate ligament (PCL), medial collateral ligament (MCL), and the lateral collateral ligament (LCL). The ACL and PCL are attached directly between the femur and tibia. The PCL prevents anterior movement of the femur along the tibia [11] while the ACL prevents anterior and rotational movement of the tibia [12]. The MCL and PCL provide stability [13], preventing medial and lateral translation. The bones and ligaments are shown in Figure 2.3.

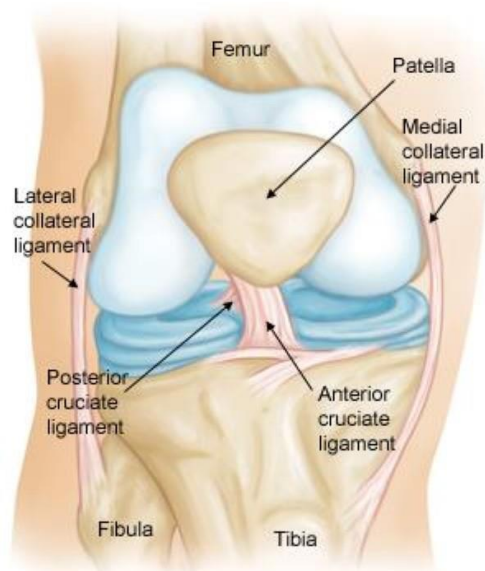


**Figure 2.3: Bones and ligaments of the knee joint. [14] Reproduced with permission from OrthoInfo. © American Academy of Orthopaedic Surgeons.**

<https://orthoinfo.org/>

Landmarks are important points on the bones that are used in total knee arthroplasty to plan and perform the procedure. The landmarks relevant to this thesis are discussed below.

### 2.1.1 Femoral Landmarks

The distal end of the femur is composed of two condyles which are hemispherical [11] and have a groove running between them. The femur center (FC) is the center of the intercondylar notch [15], or the femoral canal entry point [16]. Whiteside's Line (WS) is the anterior-posterior axis and can be defined as the line between the deepest part of the trochlea groove to the posterior projection of the femur center [17], or from the patella groove to femur center [18]. The epicondyles are the bony protrusions on the medial and lateral side of the condyles and the trans epicondylar axis (TEA) is the line drawn between them [19]. The posterior condyle axis (PCA) is the line drawn between the most posterior points on the condyles [19]. Another relevant point on the femur that is not in the distal area is the femoral head center, otherwise referred to as the hip center (HC).

This is the center of rotation (or pivot point) of the femur relative to the pelvis [20]. The landmark points are shown in Figure 2.4 and the axes that can be drawn from these points are shown in Figure 2.5.

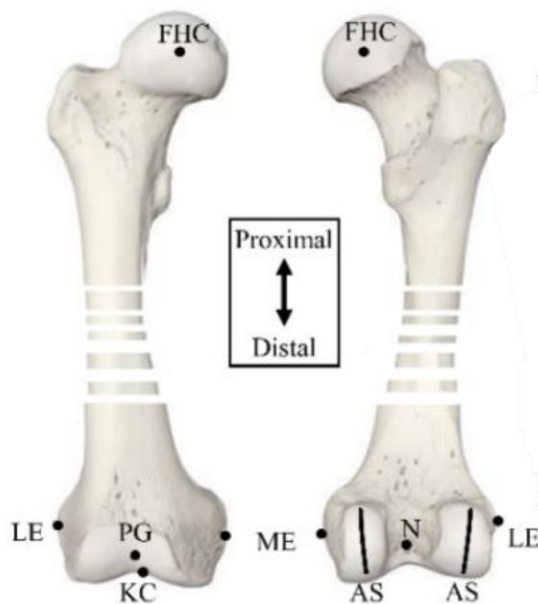


**Figure 2.4: Landmark points of the femur. KC is the knee center, referred to as the femur center (FC) in this thesis. FHC is the femoral hip center. PG is the patella groove and N is the center of the intercondylar notch on the posterior side. Whiteside's line connects these two points. AS shows the articulating surface of the condyles. LE and ME are the lateral and medial epicondyles. [17] Reproduced under the Creative Commons Attribution 4.0 International License.**

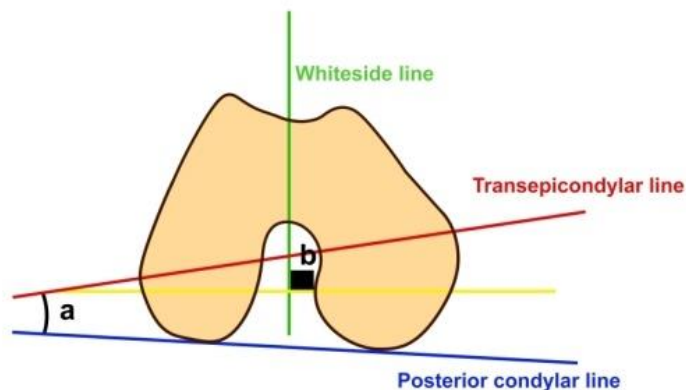


**Figure 2.5: The three axes that can be determined from landmarks on the distal femur. [21] Reproduced under the Creative Commons Attribution 3.0 License.**

### 2.1.2 Tibial Landmarks

The proximal end of the tibia is comprised of two relatively flat surfaces referred to as the tibial plateaus. The tibia center is defined as the canal entry point [16] or as the midpoint between the two plateaus [18]. The anterior-posterior axis can be defined as the line between the PCL insertion point to the patellar tendon attachment [22] or the medial third of the tibia tubercle [16]. The medial and lateral plateaus are defined as the centers of the flat surfaces discussed previously. The ankle is also used for landmarking. The lateral malleolus is the bony protrusion on the distal fibula and the medial malleolus is the bony protrusion on the distal tibia [22]. These landmarks are shown in Figure 2.6.

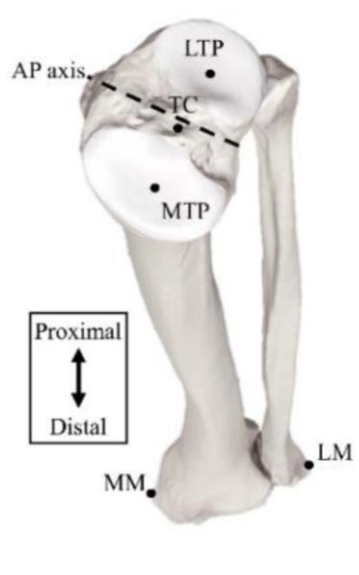


**Figure 2.6: Landmark points of the tibia. TC is the tibia center. MTP and LTP are the medial and lateral plateaus. The anterior-posterior axis is drawn with a dashed line. MM and LM are the medial and lateral malleoli. [18]Reproduced under the Creative Commons Attribution 4.0 International License.**

## 2.2 Total Knee Arthroplasty

Total Knee Arthroplasty (TKA), otherwise known as Total Knee Replacement, is a surgical procedure that aims to restore knee function and relieve pain for patients with arthritis. The surgical procedure involves resection of the femoral and tibial bones where the damaged cartilage is located [15]. First, an incision is made to expose the knee. Then measurements are taken either using instrumentation as in conventional TKAs or a computer navigation system. The surgeon then decides on the optimal position for the implant based on patient anatomy and general resection goals. These cuts are performed with the aid of a cutting guide to ensure accuracy. The surgical technique used for this thesis (and which was observed by the author as used in other systems' procedures) performs the distal femoral cut first. Then a 4-in-1 guide is used to perform other cuts on the femur to shape it to the implant [23]. The tibia involves just one proximal cut. The artificial joint is then inserted. The implants are shown in Figure 2.7. While implants vary between manufacturers, they are typically composed of a metal femoral component that



is attached to the end of the femur, and a tibial component that includes a metal component pressed into the bone and a plastic spacer above it [24].

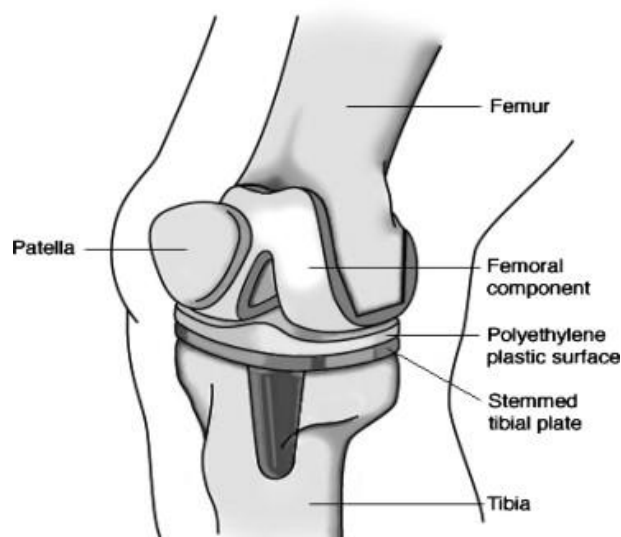


**Figure 2.7: TKA implants. Reprinted from [25] with permission from Elsevier.**

### 2.2.1 Cut Decision

In patients suffering from arthritis, their knees can be classified as varus or valgus. Valgus refers to the joint being angled laterally (the leg is “bending” inwards) and varus refers to the joint being angled medially (the leg is “bending” or bowing outwards). These concepts are shown in Figure 2.8. To ensure patient satisfaction and surgical success, the goal is to perform the resections and place the prosthesis so the knee returns as close as possible to its native alignment. Three alignment procedures can be used: mechanical, kinematic, or functional. Mechanical involves placing the implant perpendicular to the leg’s mechanical axis which runs from the center of the femoral head to the center of the ankle [3]. Kinematic alignment attempts to place the prosthesis’ joint line closer to the native joint alignment [3]. Functional alignment focuses on placing the implant to work best with the soft tissue surrounding it. The angular difference of the cut in this context is referred to as the varus or valgus angle or the cut in the coronal plane [3]. The other angle used in the first cut is in the sagittal plane and referred to as flexion angle for the femur and slope angle for the tibia. The ACL is typically removed during

the surgery and, depending on patient physiology, the MCL or LCL may need to be released to maintain balance [3]. Some computer-navigation systems and robotic systems, such as the ROSA Knee System, provide data related to the soft tissue balance of the knee [16]. The alignment procedure used is at the discretion of the surgeon. The resection depth of the cuts is dependent on how much cartilage has been lost and the size of the implant. The depth is chosen so that it matches the thickness of the implant [26].

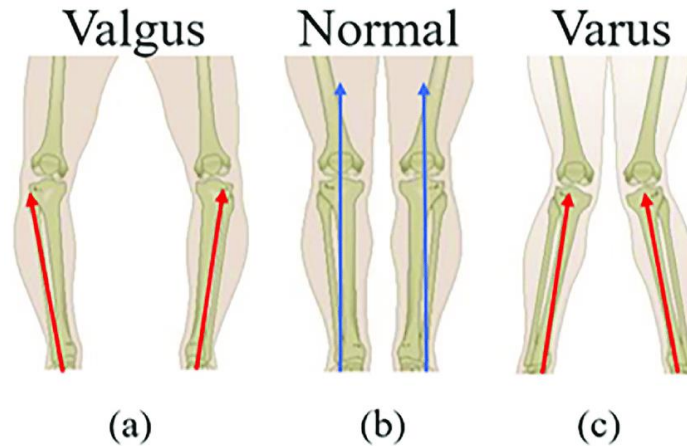


**Figure 2.8: Valgus (A), normal (B) and varus (C) leg alignment [27]. Reproduced under the CC BY License.**

Resection planning and tools for deciding implant position have evolved over many years. The conventional TKA method described in literature involves imaging the patient's leg using weight bearing radiographs. This is used to plan the angle for the femoral intermedullary guide used for positioning. Tibial alignment is typically done with extramedullary tools such as cutting guides [28] [29] [30]. However, it is possible to perform resection and alignment on both bones with either type of guide. In recent years, computer-navigated and robotic surgery has become more popular to improve implant placement accuracy.

### 2.3 Computer-navigated TKA

Surgical computer-navigated systems have shown to have several benefits in the operating room. Their main benefit is improving where the implant is positioned which leads to greater odds of the surgery being successful [31]. Navigation systems typically

involve the surgeon selecting anatomical landmarks to digitize the knee. This allows the computer to create reference frames relating to the patient's knee anatomy [32]. Surgeons then choose the depth and angle they would like for the implant and the navigation system provides live values of what values the resection would give based on where the cutting guide is currently positioned.

There are three classifications of computer-navigated systems: imageless large-console, image-based large console, and accelerometer-based [4]. The focus of this research is on imageless large-console systems. The "imageless" refers to not needing a prior imaging scan (such as a CT scan) of the patient uploaded to the system. All the data are collected intraoperatively.

In imageless-large console navigation systems, optical tracking is used to record anatomical point locations in 3D space. There are two classifications: active and passive. Active involves trackers that emit LED light that is then captured by a camera. Passive involves reflective spheres and the optical camera emitting infrared light [33]. The camera is a stereo camera, which consists of two cameras that use both images to identify points in three-dimensions. To create a reference frame on the bone for the optical system, trackers atop of bone screws are fixed into the femur and tibia respectively. It is imperative that these screws or the trackers do not move relative to the bone during surgery since landmark points are digitized in reference to them. If movement occurs for any reason, the procedure for that bone needs to be restarted. Then the surgeon uses a stylus with trackers affixed to it to select the anatomic landmarks as prompted by the computer. This allows for the optical reference frames to be related back to the knee anatomy [31]. Some landmarks are identified kinematically such as rotating the leg to find the hip center. The landmarks that are selected are specific to each system and the relevant ones will be discussed later. Once the surgeon and the computer are satisfied with the landmarks, a reference frame for each bone is created. These frames are shown in Figure 2.9.

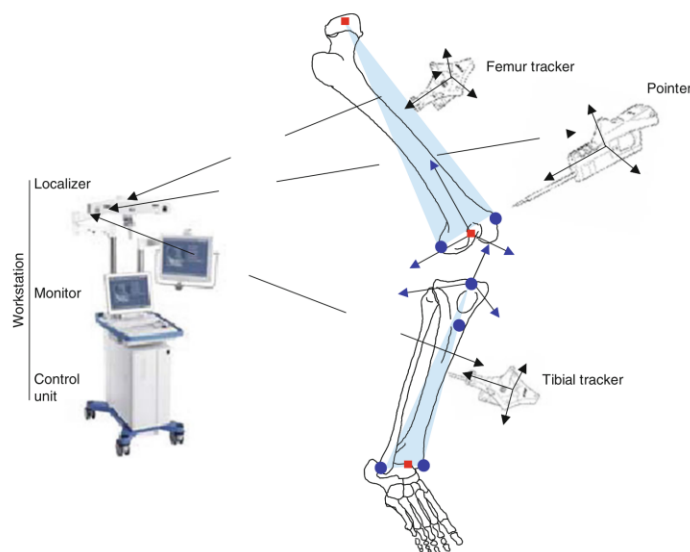


**Figure 2.9: Computer-navigated TKA equipment. The optical system is shown on the left. The trackers and pointer are shown with their reference frames. [2].**

**Reproduced with permission from Springer Nature**

The above procedure is the same for traditional computer navigated TKA and robotic TKA. Both need to register the anatomical frames of the knee before proceeding to the resection step. How they position and perform the cut on the bone is what defines the difference between the two types of systems. Computer navigated surgery typically uses cutting guides with trackers affixed to them. They provide real-time measurements of cut parameters such as resection depth and varus/valgus angle [34]. Once the surgeon is satisfied, the cut guide is rigidly fixed to the bone and the cut is performed with a bone saw. Often, the computer-navigation system also provides a process for validating the parameters of the resection after it is performed so it can be corrected if need be. The implants are then placed. Robotic systems involve a manipulator either positioning the cut guide and the surgeon performing the resection with the saw (referred to as a robotic-semi-active solution) or the manipulator directly performs the cut itself (referred to as an active solution) [35]. No matter which way the cut guide is placed, computer-navigation is the important initial step in all technology assisted procedures. Therefore, analyzing its error is very important.

## 2.4 Errors in Computer Navigated Systems

While many agree that computer-navigated surgery has several benefits, like placing implants more accurately than conventional TKA, being more useful for patients with knee deformities, or providing benefits from prior surgery requiring plates, screws, or intramedullary rods, that does not mean that it is perfect. There are several opportunities for error to be introduced during the procedure which can have consequences on surgical outcomes and patient satisfaction. Knowledge of the potential sources of errors are valuable for surgeons because it can allow them to make decisions during the operation to improve accuracy to the best of their abilities while still ensuring the surgery happens within a reasonable amount of time.

There are a few sources of errors that are outside of the operating staff's control. These have to do with the equipment itself. As mentioned previously, tracking equipment is used to gather data. If this equipment is not calibrated correctly or there was an issue during its manufacturing, the selected points will not be accurate [2]. Furthermore, the fixed markers that are attached to the bones have the potential to move or shift during surgery which means that the optical reference frames have now changed. Some systems do account for this possibility by having the surgeon probe the fixed marker to check its relative placement and restart the procedure if displacement has occurred [2]. Other issues could include inaccuracy of the optical tracking camera or of the active/passive spheres.

Another source of potential error is during the digitization phase. It has been reported that if a surgeon has even just small inaccuracies while selecting the landmarks, this has the potential to cumulate to a negative effect with implant positioning [32]. These errors are often classified as variability of points because the surgeons do have an idea of where the correct point is but choosing the same point every time is difficult, especially when working in the order of millimeters. There have been multiple studies investigating the different landmark location choices the same surgeon will make during several trials on the same bone model [36] [37]. Yau et al [37] found that surgeons selected points up to 7.6mm away from the center of the distal femur and standard deviations from ideal points were as high as 1.5mm for some landmarks. Therefore, even well-trained surgeons can

have difficulty repeating the same landmarks over and over. Other sources of landmark acquisition error can include landmarks that are not easy to identify. It was noted by the author while observing a computer-navigated procedure that malleoli points were sometimes difficult for the surgeon to identify because of the soft tissue in the area and the wrappings that are put on the patient's leg.

When considering the importance of these errors, the effect on final implant position is the most critical factor. This means cutting guide placement since, for a purely computer-navigated system or a semi-active robotic system, the surgeon performs the actual resection with the help of the guide. A few studies have been done that investigate this. Amanatullah et al [7] performed a study investigating the "safe zone" that a landmark error could be within before impacting the final angle of the bone cutting block. For each landmark, they had the surgeon digitize a sawbone at an increasing distance away from what was considered the ideal point while keeping the rest of the landmarks correct. If the suggested cutting block position changed by more than a degree, that level of error was considered outside of the "safe zone". They found that the distal femoral epicondyles had the smallest safe zone in the anterior/posterior direction, affecting the bone cutting guide placement when selected only 2mm away from the ideal point. However, selecting those points incorrectly in the inferior/superior direction (at a maximum of 16mm) had no effect on the angle. This shows how sensitive some of the landmarks can be at specific locations. One limitation of this study is that all other landmarks were kept in the correct position while analyzing error. In a clinical situation, it is unlikely that a surgeon will be perfectly accurate on all digitizations except one, and this limitation is addressed in this thesis.

Another study by Schlatterer et al [38] created a simulated version of the digitization process to see how spherical errors of uncertainty could affect final implant position. They used a Monte Carlo method to simulate the noisy error that could be caused by the optical tracking system as well as a separate Monte Carlo to investigate how a sphere of uncertainty of surgeon-selected landmark points could affect the reference frames and implant position. They found that the potential small errors created by the optical tracking system do not have a notable effect on the outcome of the implant placement. By creating

simulated bone reference frames using simulated landmark coordinates they were able to edit these coordinates to see how the angular position of those reference frames (and ultimately the implant) changed. All landmarks were given the same diameter of uncertainty sphere for each trial simultaneously and were limited to the size of variability of that point as reported in literature. For example, the femur center, hip center, and posterior condylar points had a dispersion within a sphere diameter of 1mm and the results were calculated, then they were all increased to 2mm, etc. They found that with maximum uncertainty spheres of 15mm, the maximum angular change was in the axial rotation for the femur ( $2.37^\circ$ ) and for the tibia ( $3.84^\circ$ ), showing that landmark errors do have an effect on the bone reference frame. A limitation of the study is that the same level of uncertainty was applied to all landmark points at the same time, so the effect of each individual one was not calculated. Another limitation of both this study and Amanatullah's is that they only looked at rotation but resection depth is also an important cut parameter.

There are other studies that have investigated errors in computer-navigated TKA [32], [36], [39], [40], however, only the literature most similar to the methods and analysis in this thesis were discussed in detail. The work done by Schwarzkopf et al [40] did use the same navigation system as in this thesis' methods, but their primary objective was determining the difference between the goal cut parameters as determined by the cutting guide's placement and the results from the actual cut. They found that statistically significant differences did occur and, therefore their data could be used in combination with this thesis to give an overview of potential sources of error throughout the entire procedure.

## 2.5 Reference Frames

As mentioned previously, the registration process during a navigated TKA creates a reference frame relating the global (optical system) to the respective bone. A reference frame is used as a numerical method to define spatial relationships between objects [41]. In the case of a navigated TKA, the system needs to know where the knee is located and oriented in space to accurately place the cutting guide or the robotic arm and where important points are located on the knee.

A reference frame is comprised of 3 orthogonal axes (x, y, and z) located at an origin point. It may also be referred to as a “coordinate system” but, in the case of a TKA, this system provides a “reference” for the computer. The axes can be determined using coordinate points that are found in reference to the same object. This is the process referred to as landmarking, registration, or digitization for a computer-navigated TKA.

There are 3 general rules for establishing a reference frame [42]:

- Must be found using a minimum of 3 points.
- Those 3 points must not be collinear.
- Axes are related orthogonally (using right hand rule).

Different computer navigation and robotic systems may collect a different number of points, but typically their reference frames for each bone are built using similar calculations which are discussed below.

### 2.5.1 Femoral Reference Frame

The mechanical axis of the femur is a very common way to define a line on the bone. It is the vector found from the knee center to the hip femoral head center (referred to from here as “hip center”) [43]. The femur center, shown previously in Figure 2.4, is found by the surgeon selecting the point with the stylus. The hip center is unfortunately not as simple to acquire since it is not an exposed location during the surgery. It is found using a kinematic procedure [43] where the surgeon moves the patient’s leg through a circular range of motion. Points are captured throughout the movement from the femoral tracker and the hip center is estimated from the center of rotation of the femur [44]. The algorithms used are discussed in section 2.5.1.1. In its most simple form, the points captured from the rotation of the femur paint what is essentially the surface of a sphere with the hip center located at its center. A sphere-fitting algorithm can be used to calculate this [18].

The definition of the next axis does vary between systems depending on which points they require to be digitized but the resulting reference frames would differ slightly by



only a few degrees. One method is to use the trans epicondylar axis, which is found as the vector between the medial and lateral epicondyles [45]. Another is to use Whiteside's line, which is situated from the deepest point of the trochlear groove to the posterior intercondylar notch [46]. Either of these lines can be used for an axis because they are almost completely perpendicular to each other (an angle of about  $91^\circ$ ) [17].

Since two lines have now been defined, and it is known that all 3 axes are orthogonal to each other, the third line of the axis can be found computationally. The process to define this can be performed two different ways. The first is to project the points obtained for the second axis (the trans epicondylar axis or Whiteside's line) onto a plane orthogonal to the mechanical axis [18]. This ensures those two lines are orthogonal to each other, and then the third and final axis is found by cross product. The other method is to cross the mechanical axis and the second axis. This defines a third vector that is orthogonal to the other two that were just crossed. Then, the mechanical axis and the third vector are crossed. This redefines the line found during digitization (the second axis) to ensure it is orthogonal to the mechanical axis. The right-hand rule defines the positive direction. Both methods have the same result but the cross-product method is faster and requires less lines of calculation when used in a program like Matlab. The origin of the reference frame is defined at the knee center [18] [47]. A visualization of the femoral reference frame can be found below in Figure 2.10.



**Figure 2.10: The femoral bone reference frame from two different views. Blue is the vector from the femur center to the mechanical axis, pink is Whiteside's line, and cyan is from the right-hand rule.**

While not included in the reference frame calculation, condylar points are often also collected to define the distal end of the bone and calculate cut depth [26]. To relate the cut angle values to the femur reference frame, varus/valgus is the angular difference from the axis solved with right hand rule (the medial/lateral axis and the one shown in cyan in Figure 2.10) and flexion angle from Whiteside's line [48].

### 2.5.1.1 Hip Center Calculation

As mentioned previously, there are two main methods to calculate the hip center. The first is using sphere adjustment which involves a fixed tracker on the femur and the rotation of the leg to create a cloud of points that form the surface of a sphere. The center of that sphere is the hip center. The other is coordinate transformation which involves using biomechanical calculations to find the center point [44].

Geometrically speaking, the hip center would be located perfectly at the center of the created sphere. However, there are factors in real life that negate this statement. The main issues are that the femoral head itself is not perfectly spherical in patients with arthritis (which are the patients receiving TKAs). As well, during the surgery, the pelvis of the patient is not rigidly held in any way therefore movement can occur during the rotation. Lastly, there are errors associated with the equipment itself such as the trackers or optical

system not having an accuracy of 100% every time. This can mean a perfect sphere is not painted [49]. The coordinate transformation methods attempt to correct for these errors. One method is the pivot algorithm, which uses vector addition to relate the position of the femur to a reference frame on the pelvis [50]. Another method is least moving point which assumes the hip center is constantly moving (accounting for the second error mentioned above) and that it is the estimated center that moves the least [51]. These methods have been shown to be accurate but require both bones (the femur and the pelvis) to be tracked. Most computer-navigation systems only track the femur [20] including the ones reviewed for this thesis and so it is more likely that they are using the sphere fit method.

One point to note with the sphere fitting method is that to ensure accuracy, a large range of motion of the leg must be used [52]. Several papers describe the least-squares fitting method as the method to find the sphere center [20], [44], [53]. The equations used are shown below [54]:

$$\vec{f} = \begin{bmatrix} x_i^2 + y_i^2 + z_i^2 \\ x_{i+1}^2 + y_{i+1}^2 + z_{i+1}^2 \\ \vdots \\ x_n^2 + y_n^2 + z_n^2 \end{bmatrix} \quad (1)$$

$$A = \begin{bmatrix} 2x_i & 2y_i & 2z_i & 1 \\ 2x_{i+1} & 2y_{i+1} & 2z_{i+1} & 1 \\ \vdots & \vdots & \vdots & \vdots \\ 2x_n & 2y_n & 2z_n & 1 \end{bmatrix} \quad (2)$$

$$\vec{c} = \begin{bmatrix} x_0 \\ y_0 \\ z_0 \\ r^2 - x_0^2 - y_0^2 - z_0^2 \end{bmatrix} \quad (3)$$

$$\vec{f} = A\vec{c} \quad (4)$$

The three matrices represent aspects of the expanded sphere equation, which is rearranged in order to use the least squares method.  $x_i$ ,  $y_i$ , and  $z_i$  are the coordinate points of the femoral tracker found during leg rotation, and the  $f$  and  $A$  matrices are

composed of all points.  $x_0$ ,  $y_0$ , and  $z_0$  are the center points of the sphere and  $r$  is the radius. The least squares method is then applied to equation (1) and finds the best  $c$ .

Another method described for sphere fitting in computer navigated TKA studies is the fast geometric fit algorithm [18]. It is a non-iterative approach that is derived from a previously solved two-dimensional circle fitting algorithm. Essentially, it uses the assumption that the estimation error of the center is the difference between sphere areas and so that value is minimized for  $x$ ,  $y$ , and  $z$ . The calculations are found in the work done by Sumith [55]. It was found to be more computationally efficient and performs well against the least squares method [55]. Both processes will be applied in the methods and compared.

### 2.5.2 Tibial Reference Frame

The tibial reference frame is found in similar fashion to the femoral reference frame. Typically, the first axis (the mechanical axis) is defined between the tibia center and the center of the ankle [18]. Like the hip center point, the center of the ankle is difficult to determine intraoperatively because that area is not exposed. It can be found kinematically [56] but another reliable way is to use the medial and lateral malleoli. The center of the ankle is not the exact midpoint between these two values but instead a ratio of lateral distance from the malleoli [57]. The typical equation used [18] [19] is equation (5) below.

$$\text{Center of Ankle} = 0.57 \times \text{Medial Malleolus} + 0.46 \times \text{Lateral Malleolus} \quad (5)$$

Similar to the femoral reference frame, there are options for the next axis that is taken. One option is to digitize the anterior-posterior axis (hereafter referred to as “AP axis”) [8][22]. The other is to use the line connecting the medial plateau center and lateral plateau center [18] [47]. Again, like the femoral reference frame, two axes are known and the third can be found since it is orthogonal to the other two. The origin of the reference frame is defined at the tibial center [18]. A visualization of the tibial reference frame can be found in Figure 2.11.

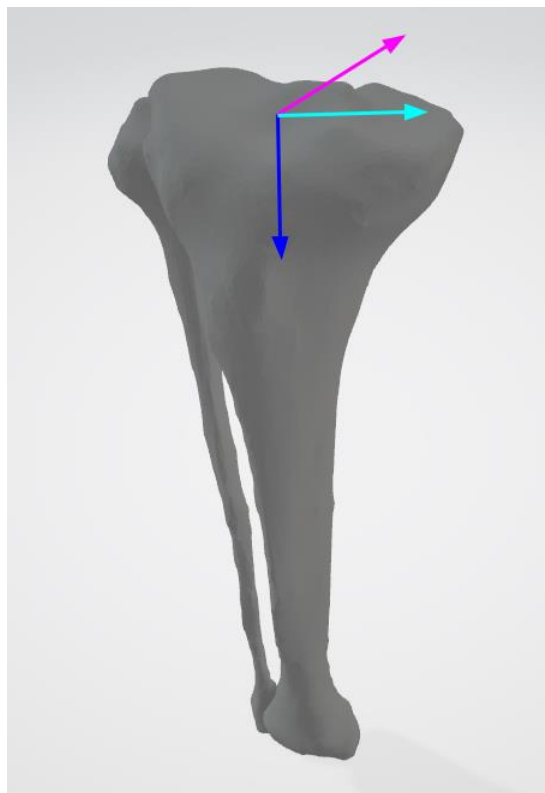


**Figure 2.11: The tibial bone reference frame. The mechanical axis from the tibia center to the center of the ankle is shown in blue. The AP axis is shown in pink. The cross between the two is shown in cyan.**

The plateau points are also collected to calculate resection depth but are not used to calculate the bone reference frame, like the femoral condylar points. To relate the cut angle values to the tibial reference frame, varus/valgus is the angle measured from the axis solved with right hand rule (the medial/lateral axis and the one shown in cyan in Figure 2.11) and the slope angle is measured as the difference from the AP axis. One way that reference frames can be easily described is with homogeneous transformation matrices.

## 2.6 Homogeneous Transformation Matrices

Homogenous transformation matrices are a representation of how an object is moved from one pose to another, otherwise known as a rigid-body motion. In robotics it is often used to describe how a coordinate system relates to a frame of reference (for example, the

pose of the end effector in reference to the camera frame). Essentially, it describes the numerical steps one would take to move from the reference frame to the target coordinate system. It consists of orientation, which is the rotation of the coordinate system, and position, which is the translation of the coordinate system [58]. A rotation matrix is of the form:

$$R = \begin{bmatrix} x_1 \cdot x_0 & y_1 \cdot x_0 & z_1 \cdot x_0 \\ x_1 \cdot y_0 & y_1 \cdot y_0 & z_1 \cdot y_0 \\ x_1 \cdot z_0 & y_1 \cdot z_0 & z_1 \cdot z_0 \end{bmatrix} \quad (6)$$

Where 0 indicates the original reference frame and 1 indicates the new rotated frame which is in reference to the original. Essentially, each value in the matrix is the cosine between the axes [58].

A translation matrix is of the form:

$$d = \begin{bmatrix} d_x \\ d_y \\ d_z \end{bmatrix} \quad (7)$$

Where each element is the distance along each axis of the reference frame that the original origin point needs to be translated to reach the new origin point.

A homogeneous transformation matrix combines these two elements. Its form is [59]:

$$p^1 = Rp^0 + d \quad (8)$$

Where  $p^0$  represents the original pose and  $p^1$  represents the transformed pose.

The terms  $R+d$  can be combined to form one 4x4 matrix which is the typical representation of a transformation matrix:

$$H = \begin{bmatrix} R & d \\ \hat{0} & 1 \end{bmatrix} \quad (9)$$

This can then be applied to equations transforming coordinate systems or singular points. The order of multiplication when solving for transformation matrices is important. For

example, equation (10) shows that pre-multiplication is to transform a frame relative to the fixed frame [59]:

$$H_2^0 = HH_1^0 \quad (10)$$

And equation 11 shows that post-multiplication is to transform a frame relative to the current frame:

$$H_2^0 = H_1^0 H \quad (11)$$

This thesis utilizes the transformation matrix that relates one reference frame in terms of another. Let  $H_B^A$  be a homogeneous transformation matrix describing the coordinate system B in reference to the coordinate system of A, which is a fixed frame, and  $H_C^A$  be a homogenous transformation matrix describing the coordinate system of C in the coordinate system of A. Let  $v^A$ ,  $v^B$ , and  $v^C$  be vectors in reference to the frames described by each of their superscripts. Then, the following equations hold:

$$v^A = H_B^A v^B \quad (12)$$

$$v^B = (H_B^A)^{-1} v^A \quad (13)$$

$$v^B = (H_B^A)^{-1} H_C^A v^C \quad (14)$$

Where equation (12) shows how pre-multiplication is used to transform a vector described in a coordinate system in reference to the fixed frame so that it is described in the fixed frame coordinate system. Therefore, equation (13) shows that the inverse of that transformation would describe a vector in the fixed frame in terms of a coordinate system in reference to the fixed. This can be extended to equation (14), which shows how a vector in a coordinate system in reference to the fixed frame can be described in a different coordinate system related to the fixed frame.

## 2.7 Metric on SE(3)

SE(3) is defined as the special Euclidean group that represents all possible rigid transforms in 3D space [60]. A metric is a measurement that can be used to compare to

results and is usually categorized as length or distance. In the case of SE(3), metrics refer to the length of the shortest displacement between two poses or rigid body motion [61]. A unique challenge when comparing homogeneous transformation matrices is that they contain both rotations, measured in degrees or radians, and translations, measured in a unit of length [62].

The metric function must meet the following conditions [62]:

$$d(H_1, H_2) = 0 \text{ if } H_1 = H_2 \quad (15)$$

$$d(H_1, H_2) = d(H_2, H_1) \quad (16)$$

$$d(H_1, H_2) + d(H_2, H_3) \geq d(H_1, H_3) \quad (17)$$

With  $H_1$ ,  $H_2$ , and  $H_3$  being different transformation matrices.

Invariance refers to a result being unchanged even when a specific mathematical operation is applied to it. Left-invariance and right invariance refers to the order with which the operation is applied. Equation (18) defines left invariance and equation (19) defines right invariance for a metric on SE(3) [62]. If both are satisfied it is referred to as bi-invariant. There are no bi-invariant continuous metric on SE(3) functions, however since this thesis uses the same method of analysis between trials selecting one sided invariance is acceptable.

$$d(H_3H_1, H_3H_2) = d(H_1, H_2) \quad (18)$$

$$d(H_1H_3, H_2H_3) = d(H_1, H_2) \quad (19)$$

A metric on SE(3) that satisfies left invariance is [62]:

$$d(H_1, H_2) = \left( \int_{\mathbb{R}^n} \|H_1 \cdot x - H_2 \cdot x\|^2 \rho(x) dx \right)^{\frac{1}{2}} \quad (20)$$

Where  $\rho(x)$  is the mass density function if a solid object is being analysed or a function that decays quickly to 0 as it moves away from the object [63].



It can be shown that when the coordinate system at the center of mass is chosen to be analysed,

$$\int_{\mathbb{R}^n} x\rho(x)dx = 0 \quad (21)$$

Then equation (20) is equal to the weighted Frobenius norm [62], [63]:

$$d(H_1, H_2) = \|H_1 - H_2\|_W \quad (22)$$

The Frobenius norm of a matrix A is defined as:

$$\|A\|_F = \left(\text{tr}(A^T A)\right)^{\frac{1}{2}} \quad (23)$$

Tr refers to the trace operator, which sums the main diagonal elements of the matrix [64]. Introducing a weight W means that the Frobenius norm of WAW or AW is taken.

In the case of the metric on SE(3), the weight includes the mass and inertia matrices in order to put emphasis on certain areas of the object. However, in the case of this thesis, the object in question is an infinite plane in space. Therefore, its mass and inertia matrices are inconsequential and can be chosen as values that simplify the equation. The easiest method is to choose values that result in the weighting being an identity matrix; therefore, everything is weighted equally and the Frobenius norm can be used instead. When restricted to SE(3) with an identity weighting matrix, equation (20) reduces to the Frobenius norm [60].

The metric on SE(3) can be applied to experimental data and simulated data which is often used in a sensitivity analysis.

## 2.8 Sensitivity Analysis

The goal of a sensitivity analysis is to investigate how an uncertainty or error of an input to a model or function affects the uncertainty or error in the output [65]. It can be a useful tool to analyze the importance of various error sources on a function where each input's influence may not be clear such as the calculation of the bone reference frames. While

not classified as a sensitivity analysis within their respective papers, works like Amanatullah et al [7] and Schlatterer et al [8] investigated the effect of landmark error on an output, whether it be cut guide positioning or reference frames and, therefore could be considered sensitivity analyses. However, both of their works have limitations and gaps that are addressed in this thesis and are discussed in Chapter 4. One form of sensitivity analysis that is performed in this thesis is the one-way sensitivity analysis. This is when one input value is given uncertainty to measure the direct sensitivity of that parameter on the output. The other form of sensitivity analysis that is investigated is the multiway sensitivity analysis which is when multiple parameters are disturbed to find the influence of the output [66]. Both of these would have importance to clinicians performing computer-navigated TKAs. A one-way analysis will represent which landmarks contribute most to the overall error and provide surgeons with an idea of which ones should have more care taken when selecting. A multiway analysis is more representative of the cumulative error that can happen during a procedure [32] since it is unlikely for a surgeon to be incorrect in selecting one landmark and perfect in selecting the others. The two methods used in this thesis to perform sensitivity analysis are discussed below.

### 2.8.1 Monte Carlo Simulation

A Monte Carlo method has been used in literature to investigate the effect of landmark errors on the bone reference frame [8]. A Monte Carlo simulation is a method of analyzing a process using randomly generated values. Typically, these are values that are artificially created using a computer in order to investigate descriptive statistic values of a process, and the process is run many times [67]. A uniform random number generator is employed to simulate various possible data points with the values falling between 0 and 1 [68]. These random numbers are then applied to whatever variable is being analyzed to ensure a representative distribution of possibilities. One such random number generator is the Mersenne Twister algorithm, which was the one used in the study investigating landmark error effect [8].

The equations to calculate a sphere of 1000 points with random numbers in Matlab are shown below [69]:

$$elevation = \sin^{-1}(2 \times rand(1000,1) - 1) \quad (24)$$

$$azimuth = 2\pi \times rand(1000,1) \quad (25)$$

$$radii = R \times rand(1000,1)^{\frac{1}{3}} \quad (26)$$

These are then inputted into the `sph2cart` function which converts spherical coordinates to Cartesian coordinates [70]. In Matlab spherical coordinates, the elevation represents the angle between a vector on a unit coordinate frame and the xy-plane. The azimuth angle represents the angle between the x-axis and the projection of the vector onto the xy-plane [71].

The Monte Carlo simulation can be applied to several different methods that analyze sensitivity. One is to represent the data as a scatter plot which is considered a graphical analysis method [72]. This shows a visual representation of the influence of a specific input by calculating the potential outputs created by the Monte Carlo simulation. Another representation is through histograms [73]. These graphs are used to visualize the shape and spread of a large amount of data [74]. The data are separated into bins of equal width and the amount of data values that fall within that bin are represented in a bar graph [75]. An example histogram is shown below in Figure 2.12.

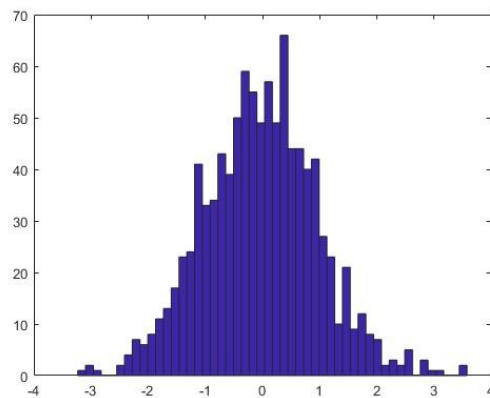


**Figure 2.12: An example of a histogram plot produced in Matlab**

### 2.8.2 Sensitivity Function using Numerical Differentiation

Another way to represent the sensitivity of a model is with a function describing how a change in input relates to a change in output, referred to in this work as a “sensitivity function”. The method to perform this involves differentiation of the model’s function. By evaluating the first-order partial derivatives of the output with respect to each input, the sensitivity is represented [72]. While there are some computer programs available that can automatically perform this differentiation, the manual numerical technique was performed in this thesis to give a greater understanding of how each input affects the function.

If the output of the system is represented by  $H$ , an input vector is represented by  $m$ , and the input is disturbed by a value  $\lambda$ , and  $f$  represents the system of equations used to solve  $H$ , it is described as:

$$H = f(m, \lambda) \quad (27)$$

With the change in input according to that disturbed value being represented as:

$$\frac{\delta m}{\delta \lambda} \quad (28)$$

Then the change of the system in response to  $\lambda$  is defined as:

$$\dot{H} = \frac{\delta f}{\delta m} \frac{\delta m}{\delta \lambda} \quad (29)$$

The  $\frac{\delta f}{\delta m}$  term in the equation is the Jacobian matrix. This calculates the first order partial derivative of the system equations with respect to each input value [76]. Its form is shown below:

$$J(m_1, m_2, \dots, m_n) = \begin{bmatrix} \frac{\delta f_1}{\delta m_1} & \dots & \frac{\delta f_1}{\delta m_n} \\ \vdots & \ddots & \vdots \\ \frac{\delta f_n}{\delta m_1} & \dots & \frac{\delta f_n}{\delta m_n} \end{bmatrix} \quad (30)$$

To write the full function showing the overall outcome by adding a disturbance:

$$H\left(m_0 + \frac{\delta m}{\delta \lambda}\right) = H(m_0) + J(H_0, m_0) \frac{\delta m}{\delta \lambda} \quad (31)$$

Therefore, by evaluating the last term in equation (31), one can evaluate the sensitivity of the system. Jacobians have been used in previous studies to analyze sensitivity of a system [77].

# Chapter 3

## Methods

The following section describes the physical data collection and the code created to simulate the reference frames created during the surgery. The equations used to analyze the data are also discussed here.

### 3.1 Physical Data Collection

#### 3.1.1 Bone Models and Mounting Structure

Two different bone models were used for digitization. The first was a medium sized right sawbone (obtained from Sawbones (Pacific Research Laboratories, Inc., Washington)) and the other was 3D printed from scans provided in a public database for a study [78] on an Ender 5 Plus printer. The dimensions of the bones are described in Table 3.1. The reason bone models were chosen as opposed to cadaveric specimens was to minimize sources of error that could come from factors other than the surgeon and the navigation system. For example, not all soft tissue around the knee is completely resected during surgery and so it can make some landmarks more difficult to identify. Using a model of just bone allowed for a completely free field of view for the surgeon to choose the points as accurately as they could. As well, this thesis also aimed to provide a workflow and methods that can be used in future research work and using artificial specimens can save on resources.

**Table 3.1: Size data for bone models used**

Bone	Femur Length (cm)	Tibia Length (cm)
Sawbone	42	38
3D print	45	39

The sawbone included the LCL, MCL, and PCL modeled with cords and held the femur and tibia together. The model did not include a fibula and so one was 3D printed and glued to the tibia. Only the bottom half was used because the only landmark point on the fibula is the lateral malleolus.

The femur and tibia of the 3D prints were attached with cords mimicking the LCL and MCL. The PCL was not needed since the goal was only to keep the bones together, the anatomical rotation of them relative to each other (which would be controlled by the PCL) was not important because each bone is registered separately. The fibula was attached in a similar manner as the sawbone.

To mimic the rotation of the femur, an acetabular cup was modeled in SolidWorks (Version 2021, Dassault Systemes, France) (shown in Figure 3.1) and 3D printed. It was designed in a similar fashion to the anatomical acetabular cup, as a semicircle in which the femoral head sat. To allow for rotation a cord was run through the bone starting at the lateral side of the femoral head, out the medial side, and through to the other side of the printed cup. This created a singular pivot point of the bone with which the hip center could then be found with a sphere fit algorithm.

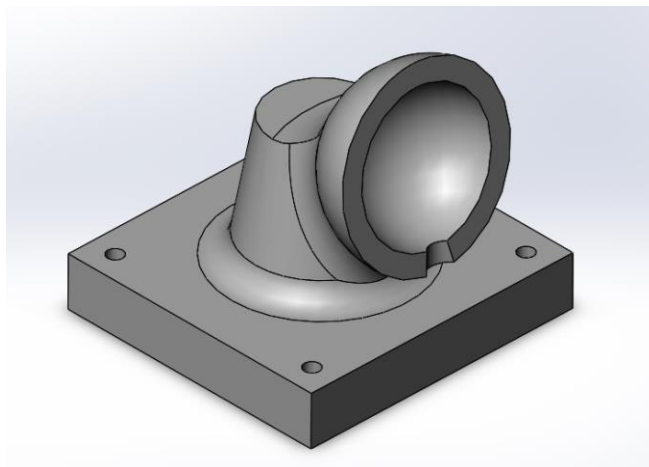


**Figure 3.1: SolidWorks part model of the acetabular cup mount**

A mounting platform for the bones to sit on during the experiments was constructed out of wood. It consisted of a horizontal piece to which the acetabular cup could be bolted. This was to ensure that it did not move during the rotation of the leg to find the hip center, eliminating another error that could be introduced during the clinical procedure [44]. It was bolted at about a 45° angle to ensure the relationship between the femur and pelvis mimics normal anatomy [79]. A vertical piece of wood was attached at about a 90° angle to the horizontal piece. This allowed for the bone to be clamped using trigger clamps so it stayed in place throughout the digitization process. This vertical piece could be removed during the rotation step to allow for full range of motion. While it was not imperative that the bone remain in the same location throughout the experiment, clamping allowed for less people to be present since the bone did not need to be held. It also helped to secure the bone when the pins were being drilled in. An anti-slip mat was placed beneath it and C clamps were used to minimize mount movement on the table.



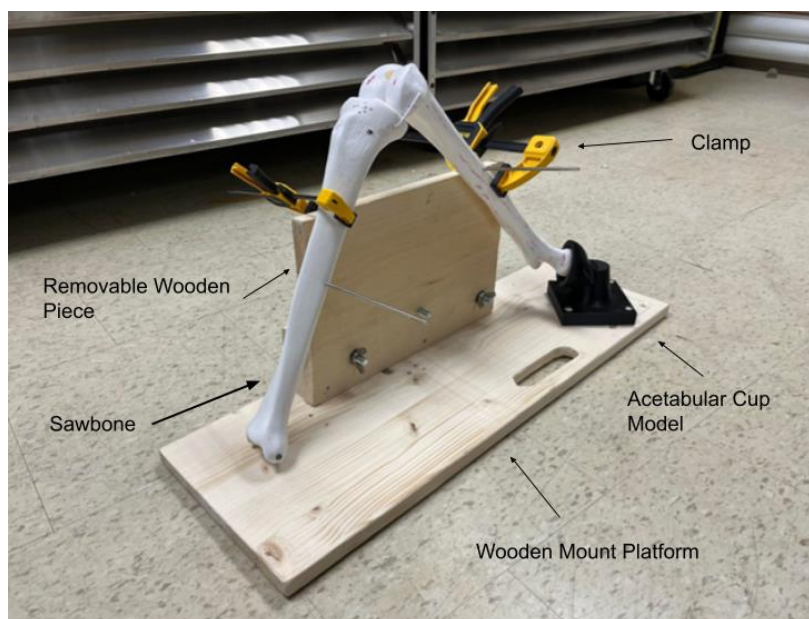


**Figure 3.2: Mounting structure for the knee joint with the sawbone mounted inside the acetabular cup model and clamped to the mount**

### 3.1.2 Intellijoint KNEE Workflow

The computer navigation system used is Intellijoint KNEE (Intellijoint Surgical, Kitchener, ON) hereafter referred to as “Intellijoint”. The system follows similar protocol to the typical computer navigation system. One unique feature is the camera used is relatively small and can be moved easily throughout the surgery versus the typical overhead camera. Also, the system works with any brand of cutting guide. The workflow used to obtain a cutting guide placement on the bone models with the Intellijoint is as follows [80]:

1. Bone screws were placed into both the femur and the tibia in an area of the bone that would be exposed during resection. In the case of this experiment both screws were placed slightly medial on the bones at the discretion of an experienced surgeon.
2. A bone tracker was installed onto the femoral screw. The femur digitization and cutting guide placement was performed first.

3. The camera was positioned so that the tracker could be seen by the optical system.
4. The bone model was rotated for the system to capture the femur center (it was continuously rotated until the system indicated it had gathered enough information).
5. The probe tracker was used to select the femur center.
6. The probe tracker shaft was placed along Whiteside's line and its position was captured.
7. The lateral condyle was "painted" which involves drawing a line anteriorly to posteriorly until the system indicates it had gathered enough information.
8. The medial condyle was painted in a similar fashion.
9. Paddles were attached to a Stryker distal femoral cutting guide (Stryker Corporation, Michigan) with the probe tracker sliding into the paddles.
10. The femoral cutting guide was placed on the femur and repositioned until it was at the appropriate location (which is discussed later).
11. Pins were drilled into the bone to secure the cutting guide to the model.
12. The system workflow was switched to the tibia and the bone tracker was installed into the tibial screw.
13. The probe tracker was used to select the lateral malleolus.
14. The probe tracker was used to select the medial malleolus.
15. The probe tracker was used to select the tibia centre.
16. The probe tracker shaft was placed along the AP axis and its position was captured.

17. The probe tracker was used to select a point (shown on the workflow screen to be in about the middle) on the lateral plateau.
18. The probe tracker was used to select a point (shown on the workflow screen to be in about the middle) on the medial plateau.
19. Paddles were attached to a Stryker tibial cutting guide with the probe tracker sliding into the paddles.
20. The tibial cutting guide was placed on the femur and repositioned until it was at the appropriate location (which is discussed later).

The optimal cut values were decided by the first surgeon performing the experiment and were set to be the values shown in Table 3.2. A visualization of what these values are referring to on the distal femur is shown in Figure 3.3.

**Table 3.2: Cut value goals.**

	Varus/Valgus (coronal plane) (°)	Femur flexion/tibial slope (sagittal plane) (°)	Lateral depth (mm)	Medial depth (mm)
Femur	4	0	9	7
Tibia	4	0	2	2

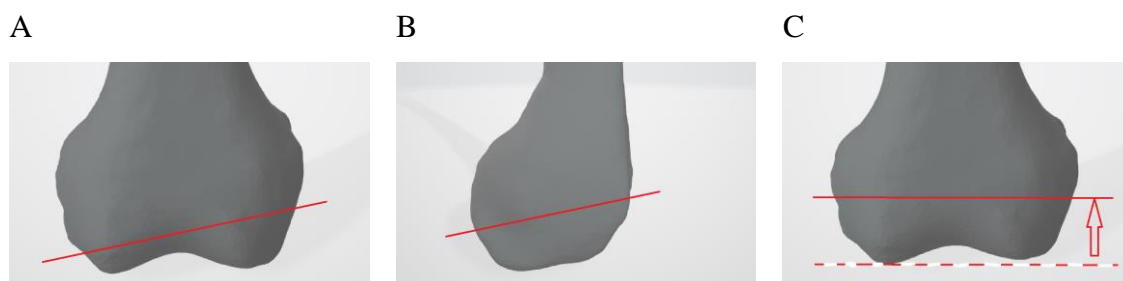


**Figure 3.3: A. Varus/valgus cut on distal femur. B. Flexion cut on distal femur. C. Depth resection on distal femur.**

### 3.1.3 Optotrak Certus

The Optotrak Certus (Northern Digital Inc., Waterloo, ON), hereafter referred to as “Optotrak”) can be used to capture real-time motion of an object. For these methods, it was used to replicate the points taken during the navigated surgical workflow. Both transformation matrices and single 3D points can be obtained by the system. It has an accuracy of up to 0.1mm and a resolution of 0.01mm [81]. The system consists of a camera (Figure 3.4) placed at about six feet away from the object being tracked. Rigid trackers which emit infrared light are mounted to the item being tracked using screws. In the case of this experiment there was one screw in the femur and one screw in the tibia. A stylus is also used to select single points on the object. These trackers and the stylus are shown in Figure 3.5. The transformation matrices of these trackers can be captured relative to the global reference frame or they can be used to provide a reference frame for other trackers. In the case of this experiment, the transformation matrix of the rigid tracker on the femur was used to capture the femoral rotation. The stylus was used to capture probed points and was in reference to the femur tracker when digitizing the femur, and in reference to the tibia tracker when digitizing the tibia. This is so that the bone could move throughout the experiment. When collecting single points from the stylus, it captured them at a rate of 10 samples/sec so what would be a singular point is a collection of points. To account for this, the average of the x, y, and z values were taken.



**Figure 3.4: Optotrak Certus camera**



**Figure 3.5: Infrared emitting trackers (encased in white) that mount onto bone screws and the stylus for the Optotrak Certus**

### 3.1.4 Data Point Collection

Point collection was performed by two surgeons experienced with navigated TKAs using the Intellijoint and the Optotrak concurrently. Rotation of the femur was able to be captured with both systems at the same time. This was done by the Optotrak using a transformation matrix that related the rigid tracker on the femur to the global reference frame (the camera) at each point in time. The x, y, and z points of the tracker's location in space were taken from the translation matrix of the transformation matrix and refers to

the tip of the pin holding the rigid tracker. Singular points, such as the femur and tibia centers, were selected by the surgeon holding both the tip of the Intellijoint probe tracker and of the Optotrak stylus at the same point on the bone. Therefore, the point registered by the Optotrak was as close as possible to the point registered internally by Intellijoint. For line selection of Whiteside's and the tibial AP axis, a custom line tool was designed and 3D printed, shown in Figure 3.6. The curved cut was placed along the shaft of the probe tracker, and the stylus drew along the rectangular groove. Since orientation of the line was important and not position, the drawn line did not have to be exactly on the probe tracker, just drawn in the same direction. For the condyles, because it was difficult to paint at the same time holding both the probe tracker and the stylus, the surgeon first drew a line with a dry erase marker. They painted along that line with the Intellijoint probe and then the Optotrak stylus. The line drawn with marker was wiped off and redrawn for each subsequent trial.

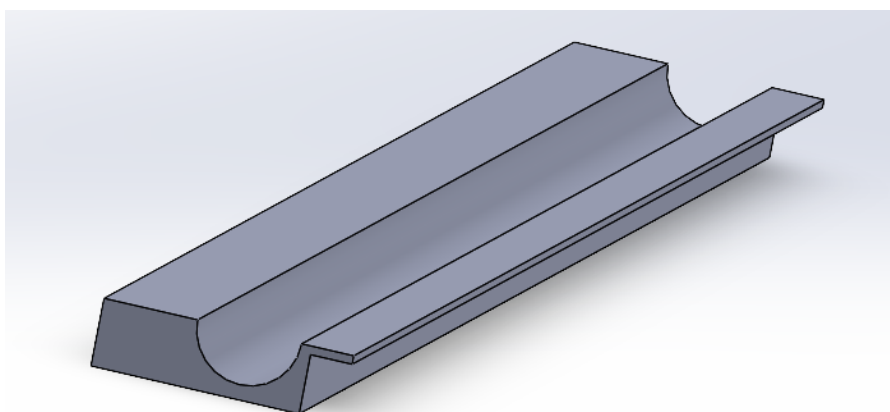


**Figure 3.6: SolidWorks part model of tool used for tracing a line along the probe tracker**

To capture the cut plane determined by the cutting guide, the saw blade (Hal 50, CONMED Corporation, Florida) was placed inside and held in the saw by the surgeon as if they were to begin cutting. Another person then painted the surface of the saw blade, creating a cloud of points that represents the cut plane. This allowed for analysis of the cutting guide position only so that errors from the actual cutting method were excluded.

Also, it allowed for the same bone model to be reused for several experiments. Experimental set up showing some pieces of equipment is shown in Figure 3.7.

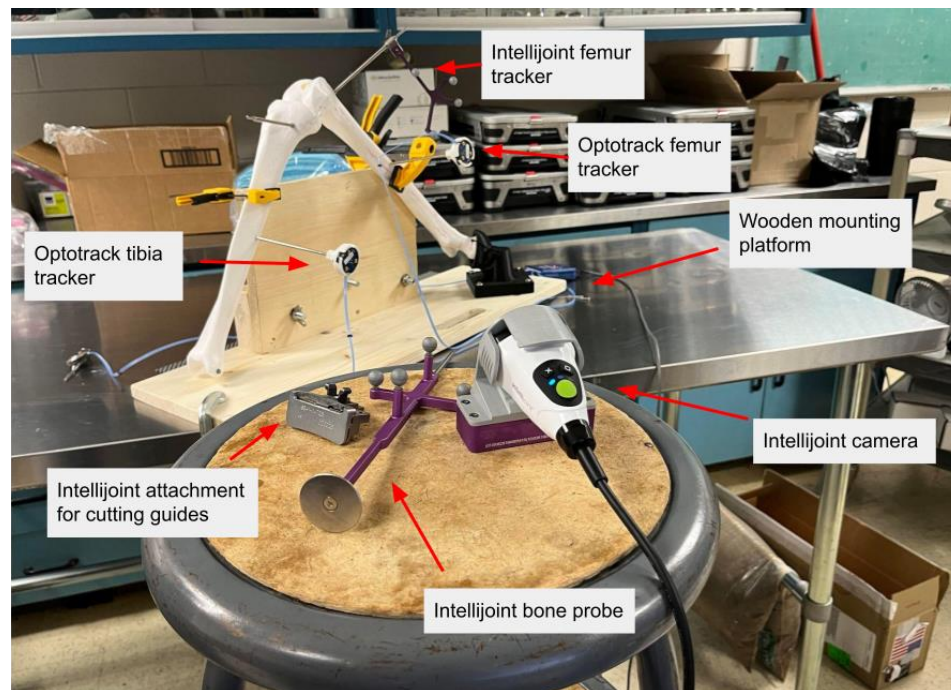


**Figure 3.7: Experimental set up for data collection.**

## 3.2 Reference Frame and Cut Plane Calculation

### 3.2.1 Femoral Reference Frame

The digital representation of the femoral reference frame was calculated using Matlab (MATLAB version: 9.2.0 (R2022a), The MathWorks Inc., Massachusetts). The hip center points were calculated according to the algorithms discussed in section 2.5.1.1 and compared. First the least squares method was used. This was implemented using a script from Jekel [54] written in Python. Then the fast geometric sphere algorithm was used. This was a script from Sumith [55] and written for Matlab. For three experiments, the resulting hip centers were compared, and all were within a Euclidean distance of 1.27mm of each other. The individual values can be found in Appendix B. As seen later, the hip center landmarks had large variability between experiments and so a difference of about a millimeter between the two methods was deemed insignificant. Therefore, either method could be used. The fast geometric sphere algorithm was chosen because it was easy to

integrate the function with the rest of the code written in Matlab. The hip center point was in reference to the global reference frame but the rest of the chosen points were in reference to the femoral tracker, so the point needs to be transformed. To do so, one of the transformation matrices of the femoral tracker (FT) calculated during data collection was chosen, and its inverse multiplied by the hip center point.

$$HC^{Femur} = FT_{Femur}^{Global^{-1}} \times HC^{Global} \quad (32)$$

The collection of points that made up Whiteside's line and the AP axis was not a perfect line and so a line of best fit was calculated. Singular value decomposition was used and the equations are below. First, the average points of the cloud are calculated which is what the line will be centered around, shown in equation (33). Then, the residual is calculated by subtracting the mean from each point, shown in equation (34). Lastly, singular value decomposition is performed using the calculated residuals. The general form of SVD is shown in equation (35), with M representing a general matrix. The matrix used for calculating the equation of the line is U in equation (35), which is a square matrix of the row size of the covariance matrix, and whose values are the orthonormal eigenvectors of the covariance matrix multiplied by its transpose. A variety of MathWorks and StackExchange forum answers were used to create this code [82]–[84].

$$(\bar{x}, \bar{y}, \bar{z}) = \frac{1}{n} \sum_{i=1}^n (x_i, y_i, z_i) \quad (33)$$

$$(x_i, y_i, z_i) = (x_i, y_i, z_i) - (\bar{x}, \bar{y}, \bar{z}) \quad (34)$$

$$M = USV^T \quad (35)$$

Now, there was enough information to calculate the femoral reference frame. The x axis was defined as the vector from the femur centre to the hip centre. The y axis was defined as Whiteside's line and these two were crossed to find z. Then, x and y were crossed to redefine y, as discussed in 2.5.1.

$$\vec{X} = HC - FC \quad (36)$$



$$\vec{Y}_{original} = WS \quad (37)$$

$$\vec{Z} = cross(\vec{X}, \vec{Y}_{original}) \quad (38)$$

$$\vec{Y} = cross(\vec{Z}, \vec{X}) \quad (39)$$

After finding the unit vectors, these vectors represent the reference frame of the femur and adding the femur center coordinate points will translate its origin to that location. A visual representation is shown in Figure 3.8.

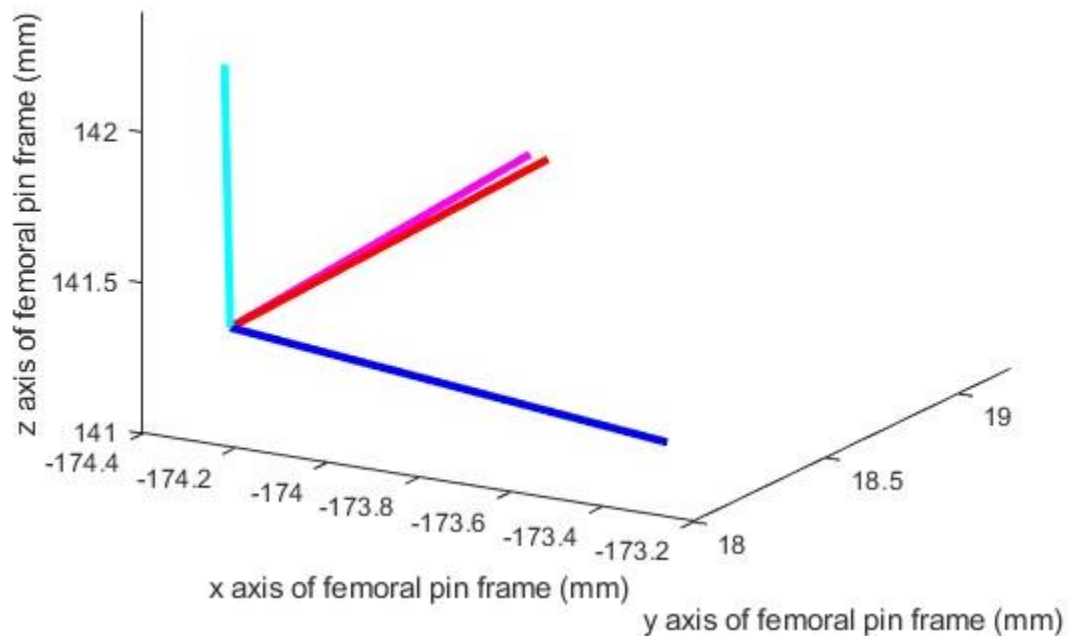


**Figure 3.8: The femoral coordinate system shown in reference to the pin coordinate system with origin at the femur center. The blue line is the bone x axis (mechanical axis), pink is y axis (Whiteside's line after correction) and cyan is the z-axis (found by crossing the other two). The original Whiteside's line vector is shown in pink.**

### 3.2.2 Tibial Reference Frame

The calculation of the tibial reference frame was very similar to that of the femur. The line of best fit calculation for the AP axis was discussed in the section above. As well, the

ratio for the malleoli points was discussed in 2.5.2. The equations to calculate the reference frame are as follows:

$$\vec{X} = (0.57 \times MM + 0.46 \times LM) - TC \quad (40)$$

$$\vec{Y}_{original} = AP \quad (41)$$

$$\vec{Z} = cross(\vec{X}, \vec{Y}_{original}) \quad (42)$$

$$\vec{Y} = cross(\vec{Z}, \vec{X}) \quad (43)$$

After finding the unit vectors, these vectors represent the reference frame of the tibia, and adding the tibia center coordinate points will translate its origin to that location. A visual representation is shown in Figure 3.9.

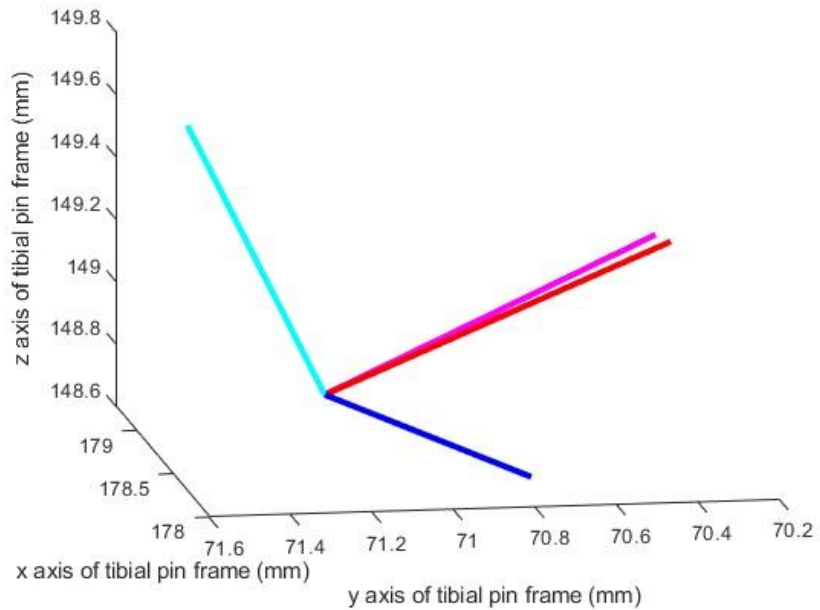


**Figure 3.9: The tibial coordinate system shown in reference to the pin coordinate system with origin at the tibia center. The blue line is the bone x axis (mechanical axis), pink is y axis (AP axis after correction) and cyan is the z-axis (found by crossing the other two). The original AP axis vector is shown in pink.**

### 3.2.3 Defining the Cut Planes

The process for defining the femoral and tibial cut planes were the same. The cloud of points collected during the experiment were read into Matlab. A function called `affine_fit` and downloaded from [85] takes a cloud of points and finds the best fit plane to them by reducing the samples by their average point and then finding the eigenvalue. The output of the equation is the normal axis to the plane and a point on that plane. The point on the plane was used to find the scalar value for the equation of the plane.

Next, the plane needed to have an origin point that was calculated in the same manner between trials to ensure the transformation matrix between the bone frame and the cut plane was being solved consistently. The origin was defined as the point on the plane that intersects the mechanical axis of each bone (x axis). A visual representation is shown in Figure 3.10.

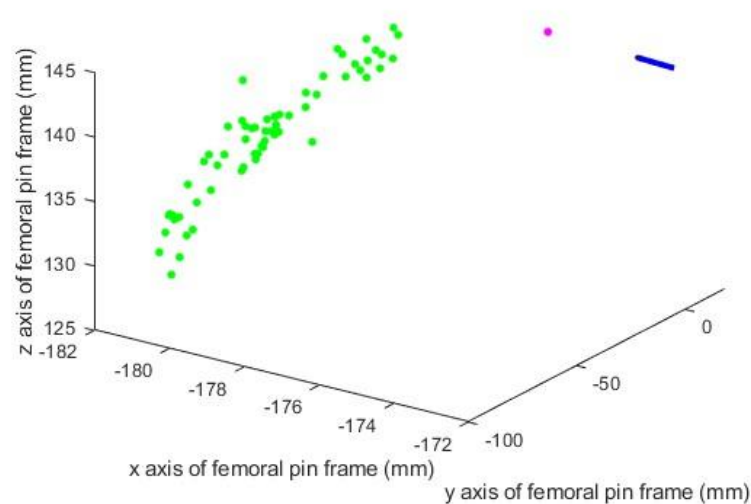


**Figure 3.10: Plot of gathered cloud of cut plane points (green), the mechanical axis of the bone with origin at the femur center (blue) and the intersection point of the cut plane and the mechanical axis (pink)**

To solve for this value, the parametric equations of the mechanical axis were defined. The scalar value was given a symbol since this would be used to solve for the point.

Those parametric equations were then substituted into the planar equation and the scalar that would satisfy the equation was solved for. Then, that scalar was substituted into the line parametric equations to determine the x, y, and z values of the intersection point. This is shown in equations (44)-(47).

$$x = FC_x + x_x t \quad (44)$$

$$y = FC_y + x_y t \quad (45)$$

$$z = FC_z + x_z t \quad (46)$$

$$Ax + By + Cz + D = 0 \quad (47)$$

Where x, y, and z are the parametric equations of the x axis and A, B, C, and D are the parameters of the cut plane.

To compare cut planes to each other, the origin point needed to be along the same mechanical axis for each trial so as not to introduce unintentional error since the mechanical axis will change between experiments. Since this origin point is being created for analysis for this work and is not an actual data point used in surgery, only its proximal/distal distance matters (not anterior/posterior or lateral/medial) because that is the variable of interest for the cut plane (how much of the bone is being resected). Therefore, the mechanical axis of the experiment with the “ideal” reference frame (discussed later) was used to solve for the origin point in every trial on that bone model when comparing cut planes to each other. Again, the origin point chosen was arbitrary since, during the actual procedure, the location of the cut guide is defined by the probe tracker position, not a point on the saw blade.

The normal vector of the cut plane was defined to be its z-axis. Again, arbitrarily chosen values needed to be kept consistent when solving variables between trials. The x and y axes of the plane are two such arbitrary values since, if they lie on the plane, their direction does not matter as long as it is calculated the same way every time the code is ran. To ensure this, the x-axis of the plane was created the same way on every bone model by crossing the z-axis with the same line every time. Then, the y-axis was solved

as the cross between the z-axis and x-axis. Figure 3.11 shows the cut plane reference frame and the bone reference frame plotted on the coordinate system of the pin tracker.

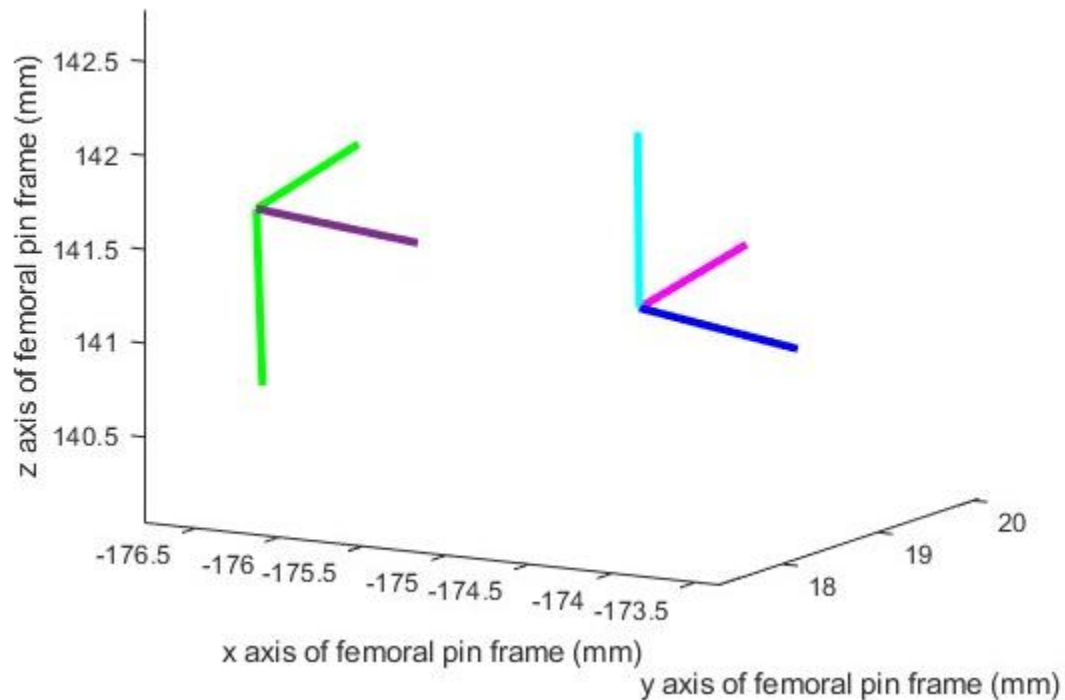


**Figure 3.11: Plot showing the bone reference frame (in the same colours as used in Figure 3.8) and the reference frame of the cut plane with the normal line to the plane (z-axis) shown in purple and the x and y axes shown in green**

### 3.3 Transformation Matrices

The transformation matrices for the femoral and tibial reference frames are already defined by their calculation above with the rotation matrix defined by the unit vectors and the translation matrix being defined by the origin (which was the femur center for the femur and the tibia center for the tibia). This was used to analyze the difference in reference frames with the variability of the selected landmarks. The transformation matrix is shown below for the femur in equation (48) and the tibia is the same except for the tibia center replacing the femur center points.

$$H_{Femur} = \begin{bmatrix} \vec{X}_x & \vec{Y}_x & \vec{Z}_x & FC_x \\ \vec{X}_y & \vec{Y}_y & \vec{Z}_y & FC_y \\ \vec{X}_z & \vec{Y}_z & \vec{Z}_z & FC_z \\ 0 & 0 & 0 & 1 \end{bmatrix} \quad (48)$$

For the cut planes, the definition of the x, y, and z vectors were discussed previously. These are used to define the rotation matrix. The translation vector depended on what was being analysed. If the transformation matrix between the bone reference frame and the cut plane was being calculated, then the translation matrix was the origin point solved for with the mechanical axis of that individual trial. If it was for comparing cut planes, then it was the origin point that was solved with the mechanical axis of the “ideal” trial. Then the transformation matrix was formed the same way as the bone matrices. This was used to analyse the difference in cutting planes. Both transformation matrices describe the position and orientation of each value in reference to the fixed tracker on the bone.

The transformation between the bone reference frame and the cut plane can be described. This is important because it is how the computer used for the navigation system would indicate to the surgeon where the cut plane has been placed relative to the bone reference frame they just digitized.

This matrix can be solved for with the following equation:

$$H_C^B = H_B^{P-1} H_C^P \quad (49)$$

With  $H_B^P$  being the transformation matrix referencing the bone frame to the fixed tracker (on the pin in the bone) and  $H_C^P$  being the transformation matrix referencing the cut plane to the fixed tracker. The resulting matrix describes the cut plane in the bone coordinate system. This multiplication order was determined in section 2.6.

The three matrices can also be related in the following manners:

$$H_C^P = H_B^P H_C^B \quad (50)$$

$$H_B^P = H_C^P H_C^{B-1} \quad (51)$$

To validate that the transformation matrix was solved correctly a few things can be done. First, one can look at the resulting translation element of the transformation matrix. The only non-zero value should be in x because the origin of the cut plane is defined as along the x axis of the bone. Also, multiplying the cut frame transformation matrix by the transformation matrix that describes the cut plane in the bone coordinate frame should result in the bone reference frame. The resulting coordinate system should have its x and y axes orthogonal to the bone reference frame z axis; therefore, the dot product should be 0. Also, the origin of the resulting coordinate system should sit on any plane of the bone reference frame (XY, YZ, XZ) to ensure it is at the origin (to check this, substitute the origin's point values into the equation of the line for any of the axes and it should equal 0).

Other points were taken with the Intellijoint protocol that contributed to the cut location but not the knee reference frame. These were the medial and lateral condyles on the femur and the medial and lateral plateaus on the tibia. These were used to determine the resection depth. The medial and lateral plateau locations were simple because they were a singular point. The condyles, however, needed to be calculated because it was a single point found along a painted line. The point used for resection depth is the most distal point [26]. In the case of this code, this would be the point furthest along the x-axis. To find the furthest point, the plane perpendicular to the x-axis was defined. The distance between the plane and each point collected during the cloud was then calculated using the following equation:

$$D = \frac{abs(ax + by + cz + d)}{\sqrt{a^2 + b^2 + c^2}} \quad 52$$

Where a, b, c, and d are the terms of the plane equation and x, y, and z are the values of each condyle point. Then the maximum distance calculated was found and defined as the most distal point for both lateral and medial, respectively. Please refer to Figure 3.12 for a plot of this.

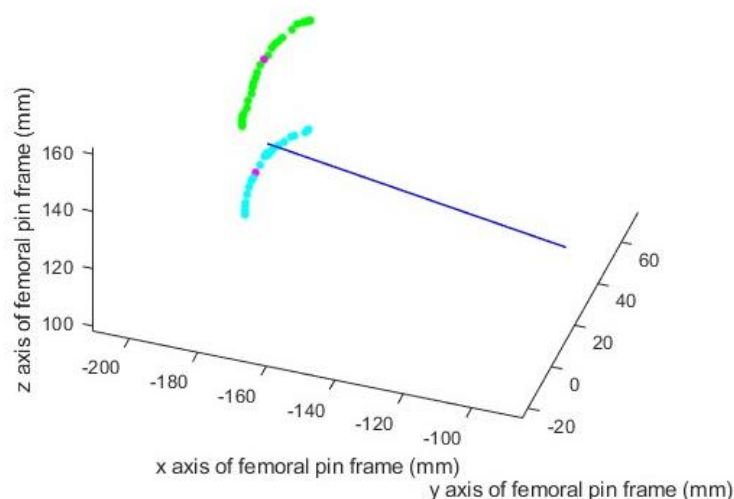


**Figure 3.12: Plot showing the collected condyle data points. The mechanical axis is shown in blue. The lateral condyle points are shown in green and the medial points are shown in cyan. The most distal point along the mechanical axis for both condyles are shown in pink.**

### 3.4 Point Error and Metric Calculation

The errors in the selected landmarks needed to be quantified to relate them to the metric on  $SE(3)$ . One limitation is that there is no “ground truth” for the landmarks, since both people selecting them were experienced surgeons choosing the landmarks without trying to introduce intentional error. To find the “ideal” trial, the mean  $x$ ,  $y$ , and  $z$  values for each landmark were found to represent the closest thing that could be considered the true point [37] and the `psearchn` function was used to find the trial with the closest values to that. This was done for each bone model. That experiment was then used to compare all subsequent trials for the metric on  $SE(3)$  errors. Theoretically, the choice of “ideal” experiment is arbitrary. It could have been any trial as long as it remained consistent throughout the analysis. However, by choosing the most ideal trial it ensures the errors are not scaled larger than they should be. Then, the error was calculated for certain landmarks using Euclidean distance in the currently analyzed trial compared to the ideal trial [37] using the `pdist2` function in Matlab, while others had a slightly different value to compare them and will be discussed in section 4.1.



The equation used for the metric on SE(3) was the Frobenius norm and can be found in section 2.7. This equation was implemented in Matlab as the following:

$$\|H_1 - H_n\|_F = \left( \text{tr}((H_1 - H_n)^T (H_1 - H_n)) \right)^{\frac{1}{2}} \quad (53)$$

Where  $H_1$  is the transformation matrix for the ideal trial, and  $H_n$  is the transformation matrix for the current trial being analyzed.

## 3.5 Sensitivity Analysis

The implementation of the two types of sensitivity analysis described in 2.8 are implemented here in regard to the landmark selection during computer-navigated TKA.

### 3.5.1 Monte Carlo Simulation

The Monte Carlo simulation was performed to analyze the sensitivity of the cutting guide placement to errors during the landmark acquisition. As mentioned previously, a sphere of erroneous points was created around each of the landmarks being analyzed with increasing radii. A MathWorks example [69] was used to create this sphere, and the equations used are discussed in section 2.8.1. The random number generator method used was the Merriam Twister algorithm, the same used in a study that also performed a Monte Carlo analysis on landmark points [8]. The center of each sphere was the landmark point from the “ideal” trial. The plot of the error sphere for the femur center with a radius of 1 mm is shown in Figure 3.13.

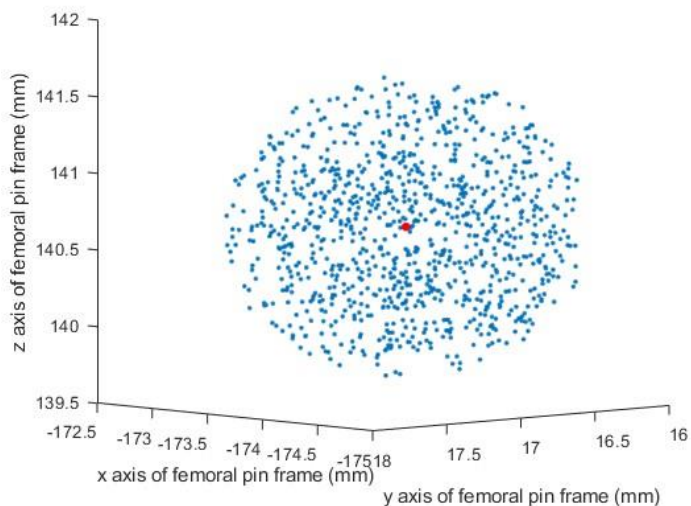


**Figure 3.13: Cloud of erroneous points used for a landmark, with the true landmark point being at the center in red.**

For each randomly generated landmark point within the sphere, a new bone reference frame was calculated using the functions created previously. To analyze a landmark individually, the uncertainty sphere was applied to that landmark and all other landmarks were kept at their ideal point. One value that was calculated slightly different than the others was the error in Whiteside's line, since that data is a cloud of points forming a line, as opposed to a singular point like the others. To apply the disturbance, the line of best fit was found with the original data. The values used to make the equation of the line were the end points of the line. Therefore, to simulate the surgeon holding the stylus at an incorrect angle, the sphere of uncertainty was applied to one of those endpoints.

### 3.5.2 Numerical Differentiation

Equation (31), which describes sensitivity of inputs using the Jacobean was implemented in Matlab. This section describes the calculation for the femoral landmark points. The workflow is shown in Figure 3.14. First, symbolic variables were defined for each point (femur center, hip center, and Whiteside's line). Since Whiteside's is a line, it had two points defined (referred to as WS2 and WS1) which represented the end points of the line. Each variable was broken down further into their x, y, and z values in order to calculate the cross product. The equations used to calculate the bone reference frame are

the same as equations (37)-(40) just broken down further to include the separate cartesian coordinate values. Each component of the x, y, and z axis were also separated into their respective coordinate values due to the cross product multiplication. The equations are shown in Appendix A. The translation vector equations were also calculated (although they were simple since they equal the femur center). Therefore, there were 12 functions and 12 variables. The Jacobian function in Matlab was used to calculate the symbolic Jacobian matrix of the bone reference frame. Since the output was very large and unrealistic to work with in symbolic form, nominal values were replaced into the function for each landmark. The values from the ideal sawbone femur trial were used. Next, symbolic variables were defined for each landmark that represented the disturbance (perturbation) to the landmark, hereafter referred to as the “delta variables”. The numerical Jacobian was then multiplied by the delta variables. Now there was a symbolic form for the equation. At this point, the norm of the matrix is calculated to have a singular equation instead of a vector. Now, the sensitivity function has been obtained and values can be substituted in for delta to check the change in output of the system. One can continue with the derivation to get the singular sensitivity coefficient for each landmark point. To do so, the Jacobian of the norm solved previously is calculated with respect to each delta variable. Now, by calculating the norm of that resulting matrix and substituting in the value 1 for one delta variable and the value 0 for all others, the sensitivity of each landmark was determined.

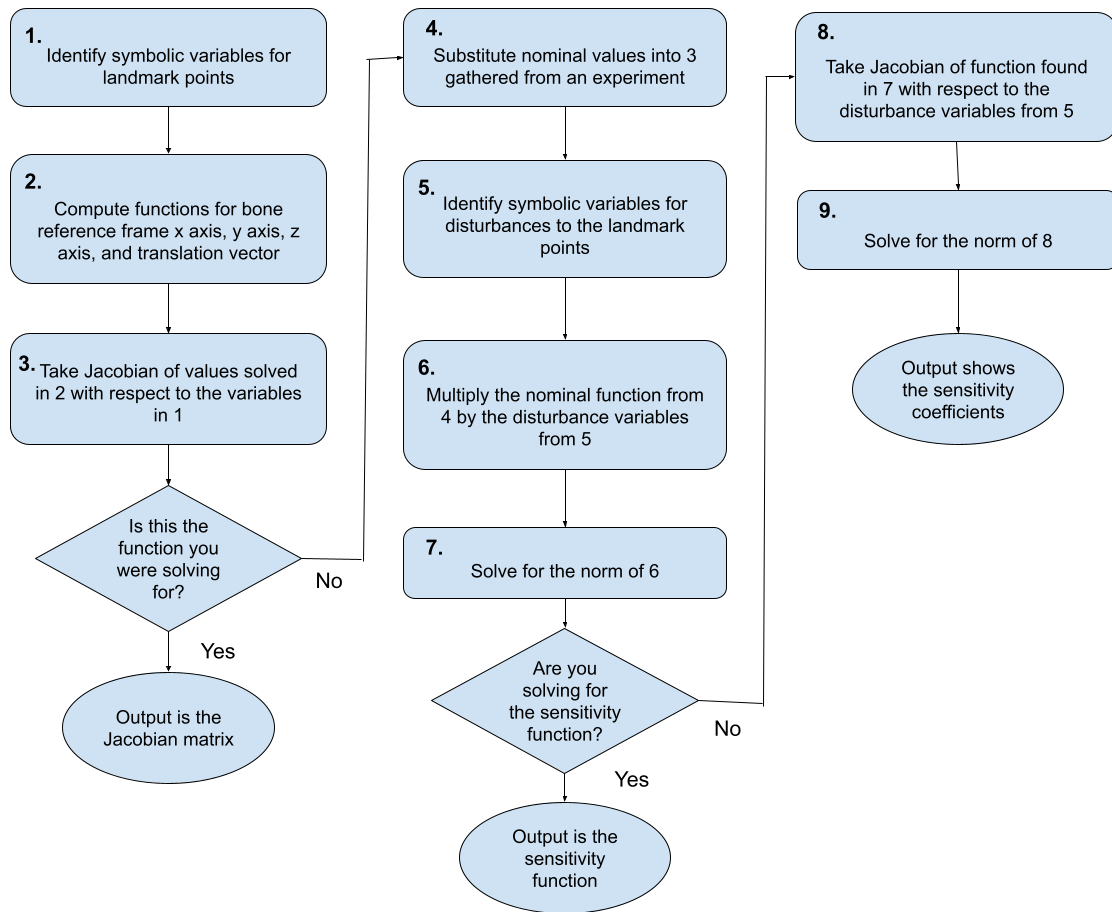


**Figure 3.14: Code workflow for the numerical differentiation method of sensitivity analysis**

## Chapter 4

# Results and Discussion

The results for the surgeon variability, metric on  $SE(3)$ , and sensitivity analysis are shown below. The implication of each section is also discussed. For bone models, SB refers to sawbone, TD is 3D printed bone, and the number following the acronym is the trial number.

### 4.1 Surgeon Variability

For one surgeon selecting points on each bone, the errors of the points are shown below. For the landmark points there is no discernable ground truth as discussed before. Therefore, the precision was measured by finding the Euclidean distance of each point from the average coordinate values for each landmark. For Whiteside's and AP axis, since they are vectors and not singular points, the error between them is the angle measured in radians compared to the average vector found for each respectively. The average error and sample standard deviation are shown in Table 4.1 and Table 4.2. Since there were 4 bone models used, the average point of each landmark was calculated individually for each bone (since they have different coordinate values) but the average overall error was calculated from the errors in both bone models (sawbone and 3D printed) in order to view what the surgeon variability was for all experiments. The individual error values are shown in Appendix B.

**Table 4.1: Femur landmark error average and sample standard deviation compared to the average point**

	Femur Center (mm)	Hip Center (mm)	Whiteside's Line (rad)	Lateral Condyle (mm)	Medial Condyle (mm)
Average	0.8028	8.175	0.05136	3.709	1.378
Sample SD	0.5038	4.416	0.01121	3.301	0.4238

**Table 4.2: Tibia landmark error average and sample standard deviation compared to the average point**

	Tibia Center (mm)	Lateral Malleolus (mm)	Medial Malleolus (mm)	AP axis (rad)	Lateral Plateau (mm)	Medial Plateau (mm)
Average	2.973	3.800	3.841	0.1431	4.843	4.210
Sample SD	1.054	1.797	2.680	0.06577	3.652	3.106

It is apparent that certain landmarks show much more variability than others. These results do differ slightly from published interobserver errors. On a nearly fully denuded cadaveric bone, it was found that the femur center and the tibia center had a mean error from the ideal point of about 1.3 mm and 1.7 mm. The same authors performed another experiment with different experimental parameters and found that the mean error for the femur center was 4.9 mm and the tibia center was 5.2 mm [86]. For this experiment, the femur center had much less variability than the tibia center (the femur center was more precise). This implies that the femur center is easier to locate than the tibia center, as is supported by literature (the tibia center error was also larger). Literature also has values

for error for the malleoli with the lateral malleolus having a mean of 1.9 mm and the medial having a mean of 0.9 mm [37]. The results found here do have higher mean errors than that. However, in the secondary study done by those authors, the ankle center, which is found as a ratio of the two malleoli (as discussed before), had a mean error of 4.9 mm [86], which is more comparable to the results shown here. A study done comparing hip center algorithm methods found that the sphere fit method, as was used here, could have precision errors as high as 35 mm. While errors did not go as high in this work, it is still the landmark with the highest average precision error and standard deviation. This could be due to the bungee cord allowing translation of the femur head inside the acetabular cup. However, this is acceptable because it mimics pelvic movement that can occur during the hip center points acquisition procedure. As of the writing of this thesis, literature could not be found about average errors for the condyles, plateaus, Whiteside's line, and AP axis. The two lines showed low variability from the surgeon, but the condyles and plateaus did show relatively higher values. However, the Euclidean distance of the points is not as important as the distance in the proximal/distal direction along the mechanical axis, since that is the direction used to calculate resection depth. The error for this is calculated in a later section. To make definitive conclusions for precision and variability, more data would be needed to ensure the sample is representative. However, for the purpose of this work, this shows that selecting landmarks can be a source of error and that it is more likely to happen with some landmarks than others.

## 4.2 Metric on SE(3)

The metric on SE(3) was used to compare several parameters. These are the difference in bone reference frames, the difference of the transformation matrices that take you from cut plane to reference frame, and the difference in cut planes. The word "error" in this section refers to the metric on SE(3) value since it is a measure of difference between two values.

When analyzing the metric on SE(3) results, it is important to remember that these values do not have a real-world unit associated with them. They are simply a scalar for comparison. They provide clinicians with an idea of how certain experiments or parameters compare to each other, but one metric value alone does not give them enough

information to determine if the output gives an unacceptable outcome to the surgery. However, by comparing values in conjunction with other variables such as landmark selection differences, one can make some estimations as to the scale of the effect that different sources of error have on the surgery.

#### 4.2.1 Bone Reference Frames

The scalar quantity representing the difference between the ideal bone reference frame for each bone and the subsequent trials are shown below. The Euclidean distance or angular difference for landmarks between the ideal experiment and the subsequent trials are also shown. A note should be taken that trials 5 and 6 were performed with a different surgeon than the other trials.

**Table 4.3: Metric on SE(3) values and landmark differences for the sawbone femur**

Experiment	Metric on SE(3)	Femur Center (mm)	Hip Center (mm)	Whiteside's Line (rad)
SB-1	1.4008	1.310	24.73	0.0315
SB-2	0.3209	0.2522	6.301	0.0819
SB-3	Ideal	Ideal	Ideal	Ideal
SB-4	0.8463	0.8437	10.55	0.0469
SB-5	1.043	1.019	20.65	0.1573
SB-6	1.674	1.650	16.502	0.1981



**Table 4.4: Metric on SE(3) values and landmark differences for the sawbone tibia**

Experiment	Metric on SE(3)	Tibia Center (mm)	Lateral Malleolus (mm)	Medial Malleolus (mm)	AP axis (rad)
SB-1	3.0868	3.0866	2.677	3.588	0.0224
SB-2	Ideal	Ideal	Ideal	Ideal	Ideal
SB-3	5.334	5.329	5.443	2.607	0.1526
SB-4	2.945	2.944	5.681	2.0644	0.0547
SB-5	11.02	11.02	3.662	7.699	0.0939
SB-6	7.626	7.625	8.653	4.352	0.0695

As one can see, certain landmarks have a much greater effect on the metric between two reference frames than others. This was slightly surprising because literature has suggested that all landmarks are important. Looking at the femur, the metric results are very low (relative to other metrics calculated later). Even with hip center error distances as great as 28.84 mm, it appears to have little effect on the metric, seeing as that trial's metric value is not the greatest. What does appear to greatly affect it is the femur center. This makes sense with how the metric is comparing the reference frames. Since it is looking at the homogenous transformation with an equal weighting, that means that the columns containing rotation values are equal to the column containing the translation. The translation is the origin, which is solely dependent on the femur center, therefore it would correlate to a higher metric error compared to the other landmarks.

With the tibia, the conclusion that the center point has the greatest effect on the error is even clearer. The metric error values are higher than that of the femur, and they are almost directly equal to the error in tibia center for most trials, no matter what the error in malleoli or AP axis was. This reinforces the idea that because the center is the origin point, it has the greatest effect on metrics in SE(3). And because the tibia had lower

precision for that landmark than the femur, it is more likely to have errors in its bone reference frame. Landmark errors are discussed further in the Monte Carlo analysis section. Metric values for the 3D printed bones were also calculated for a later analysis and are presented in Appendix B.

#### 4.2.2 Cut Planes

The scalar quantity representing the difference between the first cut plane for each bone and the subsequent trials are shown below. It is important to note that the surgeons were aiming for the same cut parameters during each trial as shown in Table 3.2 but because of the sensitivity of the system, each had to make an approximation. This is indicative of how it would occur during an actual surgery, since both accuracy and speed need to be prioritized so the patient bone is not exposed for too long, which can lead to infection. The cut parameters, including varus/valgus, flexion, slope, and resection depths are included as well.

**Table 4.5: Metric on SE(3) values and cut parameters as reported by the navigation system for the sawbone femur**

Experiment	Metric on SE(3)	Flexion (°)	Varus/Valgus (°)	Lateral Depth (mm)	Medial Depth (mm)
SB-1	0.3594	4	0	9	7
SB-2	1.452	4	0	9	7
SB-3	Ideal	5	0	9	7
SB-4	0.5184	5	0	9	8
SB-5	0.7576	4	0	10	9
SB-6	1.081	4	0	10	9

**Table 4.6: Metric on SE(3) values and cut parameters as reported by the navigation system for the 3D printed femur**

Experiment	Metric on SE(3)	Flexion (°)	Varus/Valgus (°)	Lateral Depth (mm)	Medial Depth (mm)
TD-1	4.491	4	0	8	7
TD-2	1.661	4	0	8	8
TD-3	2.536	4	0	7	7
TD-4	Ideal	4	0	6	6

**Table 4.7: Metric on SE(3) values and cut parameters as reported by the navigation system for the sawbone tibia**

Experiment and Bone Model	Metric on SE(3)	Slope (°)	Varus/Valgus (°)	Lateral Depth (mm)	Medial Depth (mm)
SB-1	0.1111	4	0	2	2
SB-2	Ideal	5	0	4	2
SB-3	0.5071	4	1 (varus)	3	0
SB-4	2.915	5	0	5	3
SB-5	2.590	4	1 (valgus)	3	0
SB-6	1.601	4	0	1	-1

**Table 4.8: Metric on SE(3) values and cut parameters as reported by the navigation system for the 3D printed tibia**

Experiment and Bone Model	Metric on SE(3)	Slope (°)	Varus/Valgus (°)	Lateral Depth (mm)	Medial Depth (mm)
TD-1	1.760	4	0	5	2
TD-2	3.740	4	0	2	1
TD-3	Ideal	4	0	4	0
TD-4	3.625	5	1 (varus)	3	1

It has been reported in literature that errors in the reference frame can have an effect on the cut outcome. To investigate this, the metric on SE(3) values for the cut planes were plotted against the values for the reference frames (Figure 4.1).

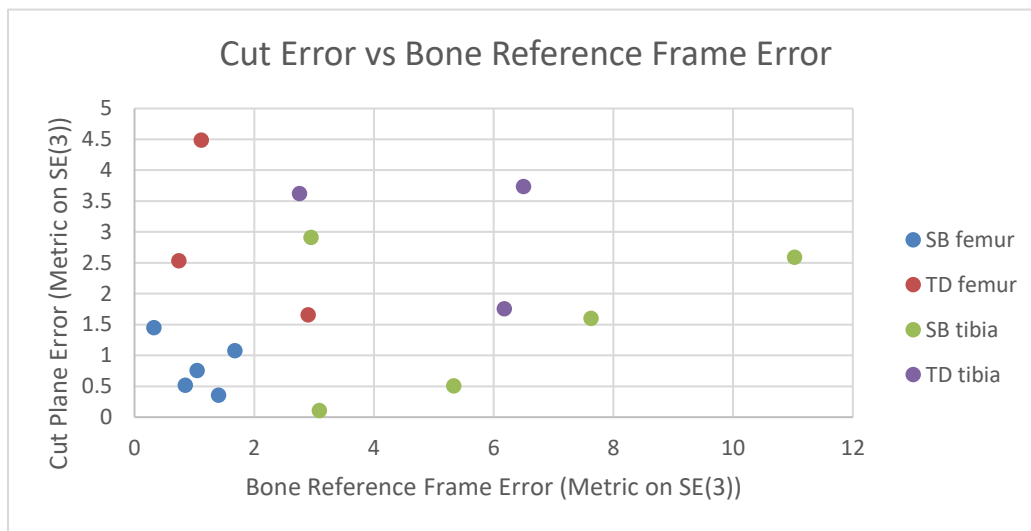


**Figure 4.1: Plot comparing the metric on SE(3) values between the bone reference frame and the cut plane**

As one can see, there does not appear to be a clear correlation between the reference frame error and the cut plane error. The largest cut plane error, which was about 4.5, was not associated with one of the largest reference frame errors (in fact, it was one of the smallest at about 1.114). The largest reference frame error also did not have an exceedingly large cut plane error. It is interesting to note that bone models appear to have certain patterns. The sawbone femur is quite clustered with small errors in both values whereas the sawbone tibia does seem to increase cut plane error with reference frame error except for one outlier. While this is not enough data to say that errors in the bone reference frame have little effect on the cut guide placement, it does show that it is not the only potential source of error.

The condyles and plateaus are landmark points that are selected for cut guide position but are not included in the calculation of the bone reference frame and, therefore, are not included in that error value. The error of the condyles and plateaus from the ideal experiment in the direction of the mechanical axis are shown in Appendix B. Again, the

distance along the mechanical axis alone matters because the resection depth is only calculated in the proximal/distal direction. For example, we can see that for SB-2 on the femur, it has a larger cut guide error than SB-1 on the femur, yet it has a smaller error in the bone reference frame. The cut parameters shown in Table 4.5 are also the same. One area where SB-2 does have a larger error that could have contributed to this discrepancy is with the lateral and medial condyles, with both points being selected more incorrectly along the distal direction than SB-1. Similarly with the tibia, SB-4 has a larger cutting guide error compared to SB-1 and SB-3, but has the smallest reference frame error. It also had the closest cut parameters to the goal values. Again, the values where SB-4 have the most errors comparatively are the plateau points. This implies that incorrectly selecting the plateaus results in a different resection depth than intended and can contribute to the error.

Another potential source of error is in the placement itself of the cutting guide. As shown above, when given goal cut parameters to achieve, the surgeons were not always able to achieve exactly those values. It was observed that the values reported on the computer screen were very sensitive to small movements done by the surgeon (a barely perceptible change in hand placement could change the angle or resection values). Since these methods aimed to see how errors could occur during surgery, the surgeons spent an appropriate amount of time (at their discretion) placing the cut guide and securing it even if it was not perfect, as opposed to spending an unrealistic amount of time trying to get the placement exact. Drilling pins into the guide also would change the cut parameters from what the surgeon had placed originally when the guide was being held by just their hand. It was noted by a surgeon that the dynamic behavior of the bone models was different than that of real bone (they vibrated more during the drilling process) which could contribute to this error but the cut guide still did move from what was originally planned. For example, TB-4 had a relatively large cut error despite it having the smallest reference frame error for the 3D printed tibia model. It did have the highest deviation in the rotational cut parameters, with a 1° larger slope and 1° difference in varus.

Interestingly, if an error is included in the bone reference frame, there is a possibility that that error could be “cancelled out” by an error in cutting guide placement. For example, if there is a 1° difference in the calculated mechanical axis, and the cutting guide is placed

with what appears to be a 1° deviation from the goal angle, that cut guide will actually be placed in the correct position relative to the ideal position.

Interestingly, there appears to be a gap in available literature on the errors in the cutting guide positioning. For example, the potential sources of error listed by Amanatullah et al [7] include things like pin placement, registration, and incorrect bone cuts but not incorrect guide placement. A book section describing sources of error for navigated TKA [2] describes issues like equipment error and variability in landmarks, but the only mention of guide positioning is that manual methods can make it more difficult to achieve the goal. It was mentioned by Figueroa et al [39] that jig placement can be placed incorrectly but their study focused on accuracy of final cuts for a robotic system. Studies that investigate the accuracy of navigated-TKAs generally appear to focus on landmark/reference frame errors or actual performed cuts compared to the planned cuts. These results show that there is an area that needs further investigation, and the point in the procedure where this error is introduced occurs between the two previously mentioned studied areas. It could also possibly show a reason why robotic-assisted TKA is beneficial. They control the cut guide placement (or in active systems, cut directly without a guide), skipping the step where error can be introduced by the surgeon placing it. However, to make a definitive conclusion on this, more data would be needed.

Overall, the cut guide errors show that when investigating procedural inaccuracies that occur pre-resection, several factors need to be taken into account, including the landmark errors, calculated bone reference frame, and actual positioning.

### 4.3 Error Cloud

Since the homogeneous transformation matrix between the bone reference frame and the cut plane was calculated for each trial, those values can provide a way to solve what would be representative of all of the possible outcomes for that set of trials. Essentially, each matrix representing the bone reference frames, cut plane, and transformation between the two can be multiplied with another one of those values using equations (49), (50), and (51) to find a new potential reference frame, cut plane, or transformation. This is because each of them was supposed to be “perfect” and in an ideal world with no

errors, be the exact same no matter which trial was multiplied by what. Since different bones appeared to have different error patterns as shown in Figure 4.1 the sawbone femur and sawbone tibia were analyzed separately originally. Each bone had 6 trials performed and since there are 3 matrices for each, 216 possible results were found ( $6^3$ ). Figure 4.2 and Figure 4.3 show all of the potential error outcomes, with Figure 4.2.A and Figure 4.3.A showing all of the points and the average, and Figure 4.2.B and Figure 4.3.B showing the density of the point clusters.

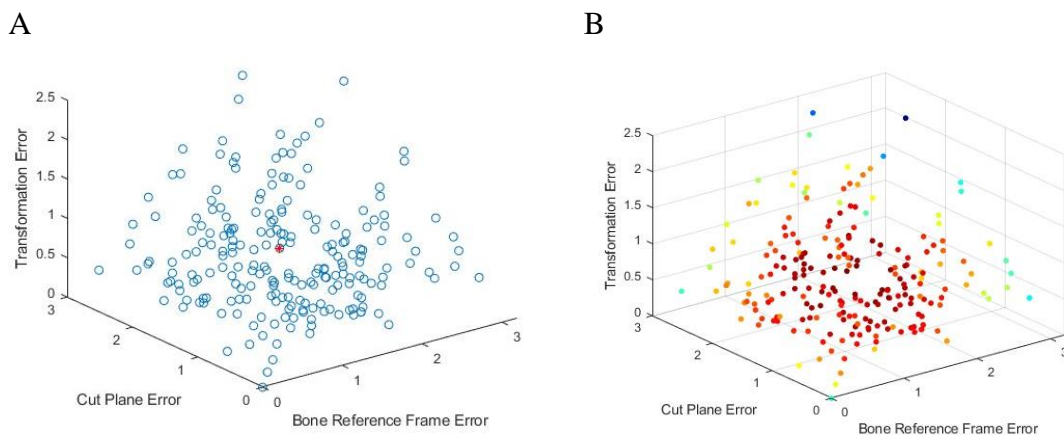


**Figure 4.2: Error cloud points for the femur. A shows the possible cloud of error points in blue, with the average point plotted in red. B shows the density of the points, with dark red being closer to the average and blue being further away.**



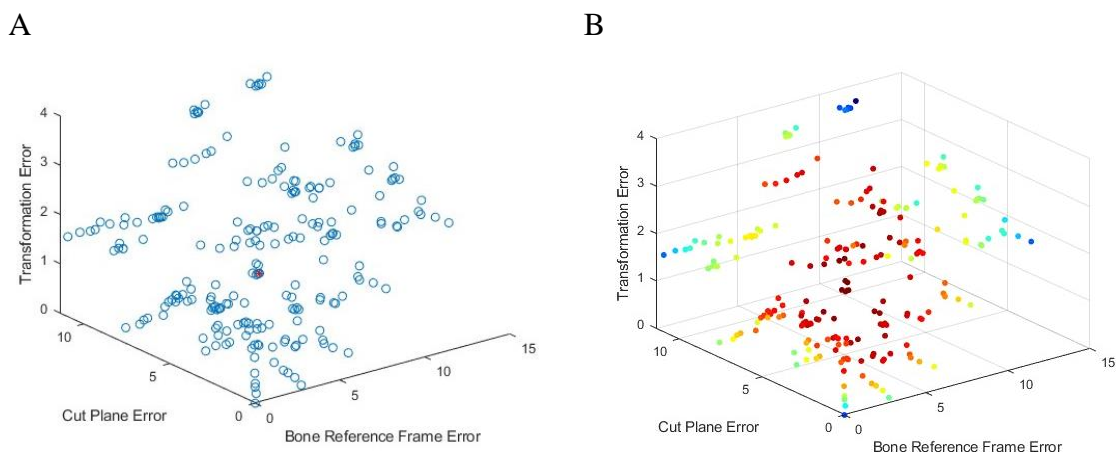


**Figure 4.3: Error cloud points for the tibia. A shows the possible cloud of error points in blue, with the average point plotted in red. B shows the density of the points, with dark red being closer to the average and blue being further away.**

Looking at the femur, one can see that the cloud of error appears to be bounded within a region of about 3 in any direction. The average potential error was 1.30 for the bone reference frame, 1.28 for the cut plane, and 0.8390 for the transformation between the two. For the tibia the range appears to be a lot larger, with the cloud stretching almost to 15 on the reference frame axis, 10 on the cut plane axis, and 4 on the transformation matrix axis between the two. The average potential error was 5.75 for the bone reference frame, 5.51 for the cut plane, and 1.60 for the transformation between the two. What this shows is that error is potentially more likely to occur with the tibia than the femur, and therefore surgeons may want to take extra care when digitizing and placing the guide for the tibia. As well, looking at the density colouring, the femur points are more clustered around the average region versus the tibia cloud being more sparse. This shows that the femur errors are generally more consistent than the tibia. It is also interesting to note that for both bone models, the average values for the reference frame errors and cut plane errors are almost equal. While this is not enough data to make a broad assumption, it could show that when looking at a larger data group than in the previous section, the

reference frame errors contribute the most to the cut plane error out of the potential error sources discussed in the previous section.

In a TKA both bones are fitted with implants. Therefore, to visualize the total potential error outcome of the surgery, the femur and tibia points for the sawbone model were combined and are shown in Figure 4.4.

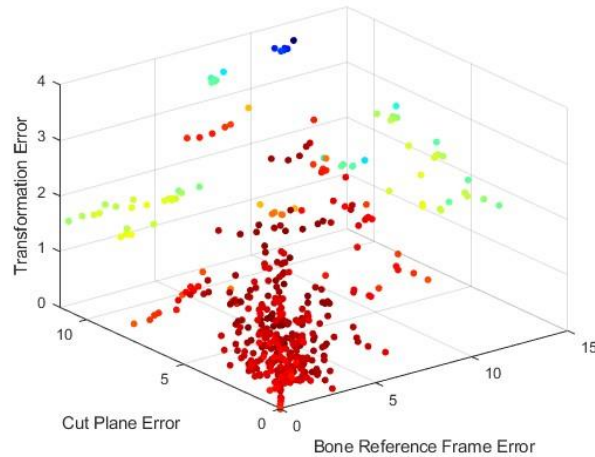


**Figure 4.4: Combined plot of the femur and tibia density errors. Points that are darker red are more clustered towards the average, and blue are further away.**

Looking at the density map, the error appears to cluster more densely in the lower area of the plot. This shows that overall outcome error is more likely to be small when considering both bones.

## 4.4 Sensitivity Analysis

The two methods of sensitivity analysis were performed for the femur and their results discussed below.

### 4.4.1 Monte Carlo Simulation

When looking at the Monte Carlo results which involve disturbing each landmark in turn and calculating the metric, it is shown how different landmarks have different effects on the reference frame errors. The results of disturbing the points within an erroneous sphere of increasing error sizes for each landmark (the other landmarks are kept at their ideal

value) are shown below in Table 4.9 along with the average metric on SE(3) value compared to the ideal reference frame.

**Table 4.9: Results from Monte Carlo simulation of the average error of the bone reference frame for erroneous spheres of increasing size**

Erroneous sphere radius (mm)	Metric on SE(3) value		
	Femur Center	Hip Center	Whiteside's line
1	0.7575	0.0023	0.0082
2	1.51503	0.0043	0.0164
3	2.2726	0.0063	0.0246
4	3.0301	0.0084	0.0328
5	3.7876	0.0105	0.0411
6	4.5451	0.0126	0.0493
7	5.3027	0.0147	0.0575
8	6.0602	0.0167	0.0658

One can see much more change with the femur center and how greatly it affects the reference frame error metric compared to Whiteside's line and the hip center points. As discussed before, this is likely due to the femur center being the origin point and, therefore, it is used in the calculation of both the rotation and translation matrices. The metric being higher for the femur center matches the results in 4.2.1 which showed that the reference frames with the higher error values were the ones with the higher center point error. The Monte Carlo experiment was run again while disturbing the femur center and only the rotation matrices compared, to eliminate the extra weighting that is happening to just the femur center with the translation matrix. The average metric was the same as the hip center points. This makes sense because they are both used to make

the x axis and, therefore, disturbing them in the same manner would result in the same outcome.

Looking at Whiteside's line compared to the hip center points, the Monte Carlo results show that errors in Whiteside's line have a greater effect on the reference frame than the hip center. This makes sense if the scale of those lines are considered. The hip center is used to create the x-axis which, before being normalized, will have a magnitude of the length of the femur. Whiteside's line in this method is created with the line tracer, which has a much smaller length than that and not always the full length was traced in the trials. However, during the actual computer-navigated procedure, Intellijoint uses the bone probe placed in the direction of the surgeon's estimate of Whiteside's line. The largest possible size the line can be is the size of the probe since the trackers are rigidly related to it, and are likely not continuing the vector past what it knows are true physical values. The length of the probe is much smaller than that of the femur. A change in position of a point further along a line than another point results in a greater change in angle from the origin, as shown in the diagram in Figure 4.5 which explains why Whiteside's has a greater effect on the reference frame.

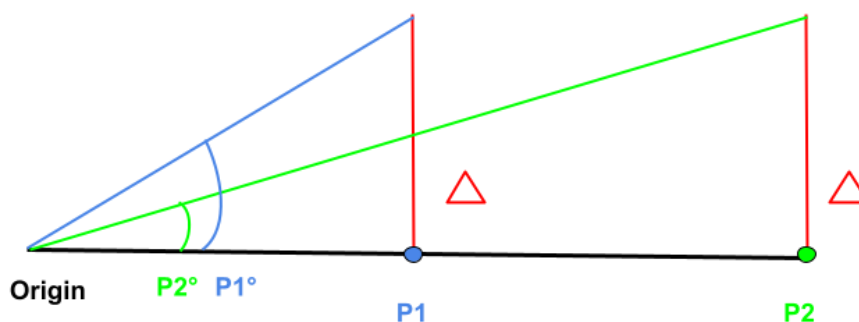


**Figure 4.5: A diagram depicting the concept of angular difference for points at different distances. P1 and P2 are two different points along the same line, with P2 being further from the origin. Both points are increased by a value of  $\Delta$ . The angular difference of the origin to the new P2 value is less than the origin to the P2 value.**

This result would also be true for other systems that instead create the secondary axis from points instead of the probe held in the vector direction. For example, the ROSA Knee System creates its PCA axis from the lateral and medial epicondyles, and Whiteside's line from the anterior and posterior trochlear groves [87]. The magnitude of each of those lines is smaller than the length of the femur.

However, these results do match one study done by Amantullah et al [7]. They found that errors in the malleoli (which are used to calculate the center of the ankle, and has the same relative function in being used for the mechanical axis as the hip center) had little effect on the final angle of the cutting guide, and concluded that points closer to the knee joint had a smaller safe-zone of error before the cutting guide position deviated too far from its ideal position.

The 1000 reference frames for each landmark error were then multiplied by the 6 transformations found experimentally between reference frames and cut plane to artificially simulate the possible cut planes, similar to what was performed in 4.3. The results are shown in Figure 4.6, Figure 4.7, and Figure 4.8 below for 1, 2, 3, and 4 mm disturbances for individual landmarks.

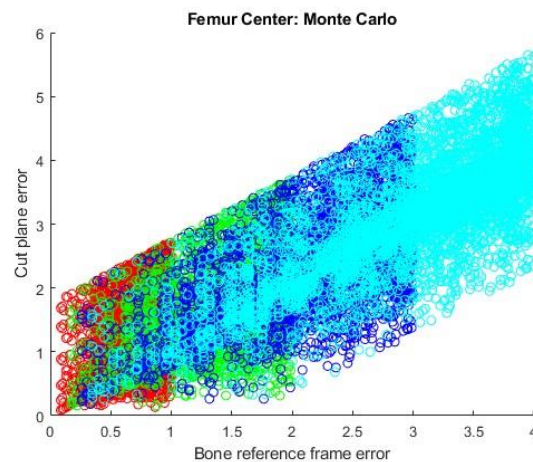


**Figure 4.6: The results of the Monte Carlo for the femur center. Red points are an error sphere of 1 mm radius, green is 2 mm, blue is 3 mm, and cyan is 4 mm.**

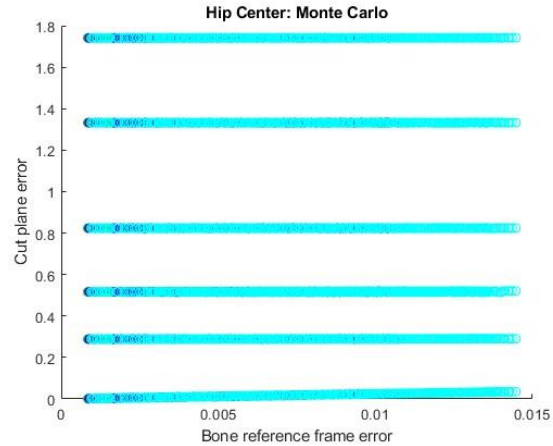


**Figure 4.7: The results of the Monte Carlo for the hip center. Red and green represent the error spheres of 1 mm and 2 mm, but they are not visible on the plot. Blue is 3 mm, and cyan is 4 mm.**

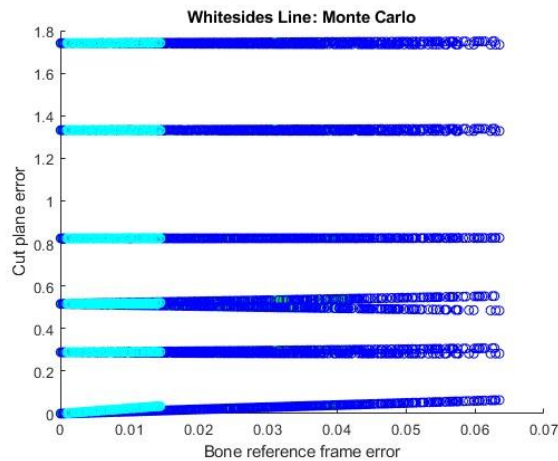


**Figure 4.8: The results of the Monte Carlo for Whiteside's line. Red and green represent the error spheres of 1 mm and 2 mm, but they are not visible on the plot. Blue is 3 mm, and cyan is 4 mm.**

The femur center appears to show a wider range of error than Whiteside's and the hip center. It is assumed that there are what appears to be 6 distinct lines for Whiteside's and the hip center because of the 6 transformation matrices by which each reference frame is being multiplied. Since the errors caused by disturbances to those two landmarks are so miniscule, the variation of the cut plane is also small and so all of the points look very

clustered on the plot. Essentially, the errors in those landmarks are being suppressed by what is assumed to be error in the cut guide positioning. Since the scale of error due to the femur center is larger, it causes the points to appear less dense than the other two landmarks. One can see that as the sphere of error around the landmark point grows for the femur center, the cut plane error becomes larger as well. To further illustrate the difference, a disturbance of 1 mm for each landmark point was plotted and shown below in Figure 4.9.

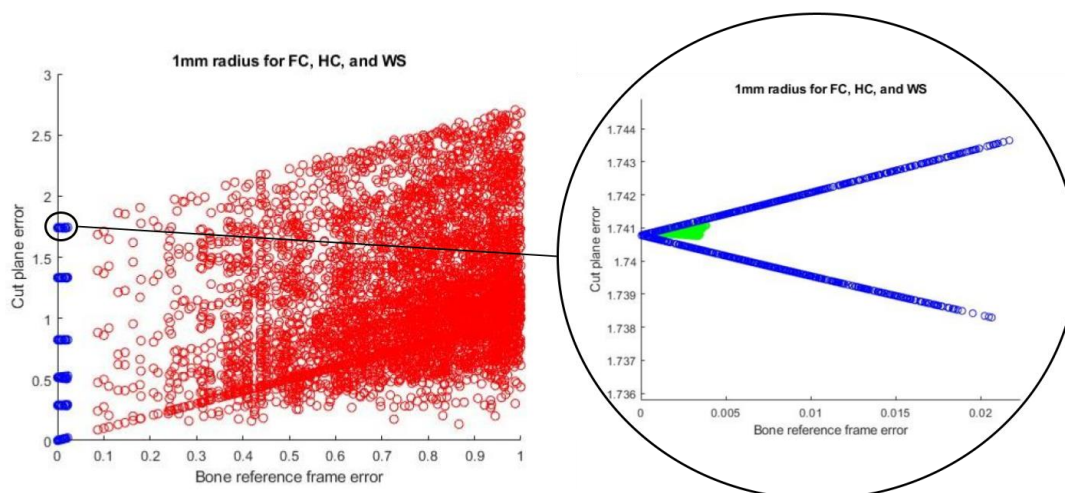


**Figure 4.9:** The plot on the left shows the Monte Carlo results for a disturbance of 1 mm of the femur center in red, Whiteside's line in blue, and hip center in green. The plot on the right is a zoomed in image so that the hip center points are visible.

Again, one can see how much larger the cloud of potential error is for the femur center compared to the blue points of Whiteside's line. When looking at the plot in full view, the green hip center points are not visible. This is because their values and deviation are so small that they are obscured by the Whiteside line points. If that area of the plot is magnified, as shown in the figure, they are visible in a small cluster.

Histograms were also produced for the cut error of the femur, shown below in Figure 4.10, showing the bins of metric values for 1 mm, 2 mm, 3 mm, and 4 mm sphere diameters. It is interesting to note that as the error sphere gets bigger, the center of the distribution moves to the right. This appears to be because the error with the highest

frequency of points is almost equal to the disturbance value and so the center of the graph will continue to increase.

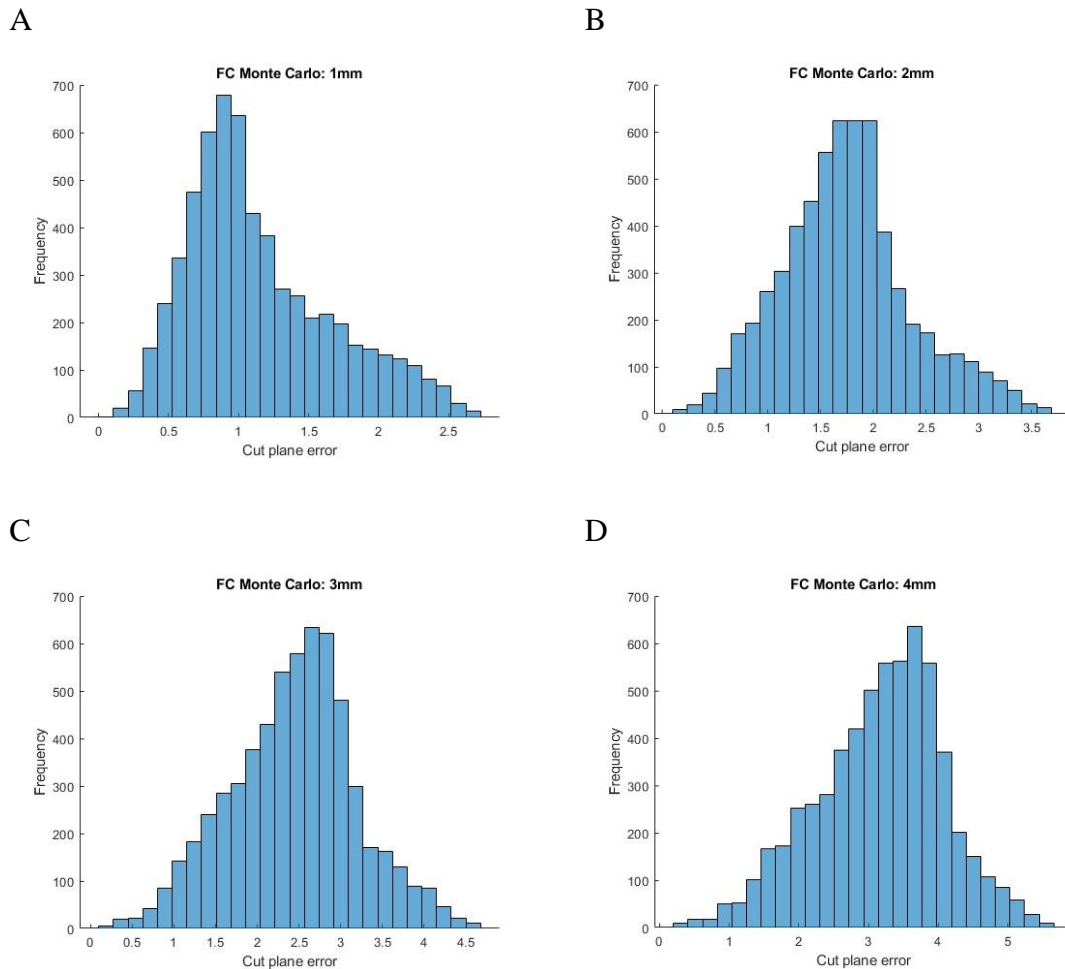


**Figure 4.10: Histogram plots of the cut plane error when the femur center is disturbed by A. 1 mm, B. 2 mm, C. 3 mm, and D. 4 mm**

As mentioned previously, a Monte Carlo simulation had already been performed in literature [8] to analyze the effect of incorrect landmarking on the reference frame. However, one major limitation of their study is that they applied the sphere of error to each landmark at the same time. This does not give specific results for each point and it is unlikely that an experienced surgeon would make large scale errors on every landmark throughout a procedure. The results found in this section provide clinicians with an idea of which landmarks should be more carefully selected than others. As well, the inclusion



of experimental data to estimate the cutting guide placement error can give a greater sense of how this artificially generated data can be applied to a real-world procedure.

#### 4.4.2 Numerical Differentiation

The numerical differentiation approach described in 3.5.2 was run in Matlab. The nominal values applied were from the ideal sawbone experiment. First, it was run to the final differentiation to get the coefficient the error is scaled by for each landmark. Each delta landmark value except the one being investigated was substituted with 0, with the delta value in question being substituted with 1. The results for each coordinate value are shown in Table 4.10. A note to add is that Whiteside's did have two landmarks associated with it (the two endpoints); however, these values were the exact same (because the two variables are just subtracted to define Whiteside's) and so only one is shown.

**Table 4.10: Sensitivity coefficients for the affect of landmarking error for experiment SB-3**

Landmark	Sensitivity Coefficient
Femur Center x	1.00
Femur Center y	1.00
Femur Center z	1.00
Hip Center x	0.0059
Hip Center y	0.0039
Hip Center z	0.0063
Whiteside's x	0.030
Whiteside's y	0.030
Whiteside's z	0.030

The results shown here match much of the results shown before, that the femur center affects the errors in the reference frame transformation matrix much more than the other two landmarks. These results also match the Monte Carlo in that errors in Whiteside's line have a greater effect than errors in the hip center, although the scale of both are still relatively small compared to the femur center. The above is a performance of a one-way sensitivity analysis (the demonstration of the effect one parameter has on the output of the system). By analyzing the outputs of the function given before the last Jacobian is performed, one can perform a multiway analysis.

The function created by stopping at Step 7 of the process in Figure 3.14 allows the user to input error values for each landmark point and see the effect they would have on the bone reference frame error (the value of the metric on SE(3)). The amount that the overall changes for each landmark contribute to the total error is by the multiplication of the

delta value by the sensitivity coefficient in Table 4.10. Table 4.11 below shows a few examples of perturbations substituted for each landmark and the corresponding reference frame error.

**Table 4.11: Various outcomes of the metric on SE(3) values (error in the bone reference frame) with varying inputs for disturbances to the landmark values**

Metric on SE(3) (Error)	Delta Value (perturbation in mm)											
	FCx	FCy	FCz	HCx	HCy	HCz	WS1x	WS1y	WS1z	WS2x	WS2y	WS2z
0.5386	0.5	0	0.2	0	0	1.7	0	0	0	2	1.8	0
2.825	0	2.8	0.4	3	1.9	0.1	2	1.6	0	0.4	0.8	1.2
0.0293	0	0	0	6.3	7.9	3.4	1.5	0.2	0.8	2.5	0.6	0
0.7097	0.3	0.4	0.5	10.4	15.6	12.6	0.5	0.3	0.2	0.7	0.1	0.4

Again, it is obvious that the femur center has the greatest effect on the error. Even when the hip center is given large errors (as was found experimentally), the errors in the bone reference frame do not scale larger in the same manner. Essentially this proves that this is a valid function for investigating reference frame differences due to landmarking errors. It is a method that can be used in future research in this area or as a tool for surgeons to understand how their specific variability in landmarking can affect the outcome of the surgery. For example, if they have access to a coordinate system capture device such as the Optotrack Certus used in this experiment, they can capture an ideal point for each landmark and substitute it into this equation. Then, after performing several trials, they can input their average variability at each point and see the effect it would have on the reference frame error. This can be used as a powerful tool for research or training purposes for computer-navigated and robotic systems.

Sensitivity analysis was only performed on the femur, but the results for the tibia would be very similar because their bone reference frames are calculated the same way. The only difference would be that the lateral and medial malleoli would affect the system with the same ratio they are multiplied by to calculate the ankle center.

# Chapter 5

## Conclusion

### 5.1 Summary

As technologically assisted TKA becomes more common in the operating room, specifically those which utilize computer navigation, it is increasingly important to understand how and why errors occur so that they can be prevented. The work in this thesis presents an analysis of the errors and a workflow that surgeons and researchers can use in the future to perform similar analysis on other systems.

Using a 3D point capture system, the pre-resection steps of a computer-navigated procedure were mimicked to produce similar data to what the system collects. A code was developed to calculate the bone reference frames. With slight modifications depending on which landmark points are used, this code can be used with other navigation or robotic systems for analysis.

By using points captured from the Optotrak, variability for one surgeon between their landmark points could be calculated. It was found that certain points were more precise than others, like the femur center versus the tibia center. The hip center was found to have the largest variability which correlates to limitations of the methods used to calculate it during the actual surgical procedure.

A metric on  $SE(3)$  was used to analyze the difference between homogeneous transformation matrices. This provided a way to apply robotics fundamentals to what is typically a more clinical-based analysis approach. It was found that the metric on  $SE(3)$

(and essentially the error) for the bone reference frames was heavily dependent on the origin points of the coordinate system which was attributed to the translation column in the transformation matrix. When comparing cut plane errors to bone reference frame errors, there did not appear to be a strong correlation between the two. This implies that there are other factors that affect the placement of the cut guide like the selection of the condyle and plateau points and the sensitivity of the cut guide parameters to small movements done by the surgeon. This analysis was extended between experiments to make a cloud of possible error points that could have occurred. It was found that the femur errors were more clustered and lower than the tibia.

Finally, two methods of sensitivity analysis were performed: a Monte Carlo simulation and a numerical differentiation to find a sensitivity function. Both confirmed what was determined before: that the landmark that provides the origin of the bone reference frame affected the error the most. It was also determined that landmarks found further away from the bone resulted in smaller errors when they were disturbed than ones closer to the bone.

These results provide important information for surgeons that could help with their accuracy and speed during the procedure. It shows that the femur center and tibia center should be selected with care, whereas procedures like the femur rotation to capture hip center do not have to be as accurate and will not affect the outcome greatly. It also shows that placement of the cut guide can contribute to the difference that occurs from the ideal cut plane. Possibly, this indicates an advantage of robotic TKAs. The code created for this thesis can be applied to future error analysis projects and to perform this error analysis on other systems.

## 5.2 Limitations and Future Work

There are a few limitations to the work presented in this thesis. Future work could involve rectifying these limitations to provide a greater scope for the results. The first is that there is opportunity for experimental error. Since the data points could not be extracted directly from the computer navigation system and, instead, had to be selected with an external system, there is no guarantee that the points being chosen were the exact

points the system sees. For singular points, the probe and Optotrak stylus were held as close together as possible but there is no way to have them touch the exact same point. For Whiteside's line and the AP axis, the line tracer tool helped ensure the stylus was drawing a line in the general correct direction but a line of best fit still had to be applied while, for the surgical system, it is assumed it is an equation with a rigid relationship with the probe. To improve this, one could work directly with the corporations providing these systems to use the true points that the optical system captures.

Another limitation of this study is the amount and variation of data. Therefore, the major next step for this work would be to evaluate a wider variety of experiments. Most of the trials were done with the same surgeon and 4 bone models were used. To be able to draw more concrete conclusions, having multiple surgeons perform the same experiment will give greater sense of interobserver variability. As well, every patient's bone is slightly different. This study could be expanded to include more deformed bones to represent that patient population. As well, analyzing cadaveric bones could show the influence of soft tissue on the errors.

The primary next step of this work is to apply these methods to other computer-navigated and robotic systems, specifically ones that take different landmark points to compute the reference frames or systems that have a different procedure of placing the cutting guide. This can help determine which reference frame system calculation is superior at minimizing errors caused by landmarks, as well as a quantifiable value to see if the robotic manipulator method of positioning the cutting guide is more beneficial than manual surgeon placement.

## References

- [1] E. M. Badley, C. M. Goulart, D. B. Millstone, and A. V. Perruccio, “An update on arthritis in Canada - National and provincial data regarding the past, present, and future,” *Journal of Rheumatology*, vol. 46, no. 6, pp. 579–586, 2019, doi: 10.3899/jrheum.180147.
- [2] A. Leardini, C. Belvedere, A. Ensini, V. Dedda, and S. Giannini, “Accuracy of Computer-Assisted Surgery,” *Knee Surgery Using Computer Assisted Surgery and Robotics*, pp. 3–20, Jan. 2013, doi: 10.1007/978-3-642-31430-8\_2.
- [3] S. Oussedik, M. P. Abdel, J. Victor, M. W. Pagnano, and F. S. Haddad, “Alignment in total knee arthroplasty,” *Bone and Joint Journal*, vol. 102 B, no. 3, pp. 276–279, 2020, doi: 10.1302/0301-620X.102B3.BJJ-2019-1729.
- [4] C. W. Jones and S. A. Jerabek, “Current Role of Computer Navigation in Total Knee Arthroplasty,” *Journal of Arthroplasty*, vol. 33, no. 7, pp. 1989–1993, 2018, doi: 10.1016/j.arth.2018.01.027.
- [5] K. A. Ross, D. H. Wiznia, W. J. Long, and R. Schwarzkopf, “The Use of Computer Navigation and Robotic Technology in Complex Total Knee Arthroplasty,” *JBJS Rev*, vol. 9, no. 5, May 2021, doi: 10.2106/JBJS.RVW.20.00200.
- [6] C. H. Yan, K. Y. Chiu, F. Y. Ng, P. K. Chan, and C. X. Fang, “Comparison between patient-specific instruments and conventional instruments and computer navigation in total knee arthroplasty: a randomized controlled trial,” *Knee Surgery, Sports Traumatology, Arthroscopy*, vol. 23, no. 12, pp. 3637–3645, Dec. 2015, doi: 10.1007/s00167-014-3264-2.
- [7] D. F. Amanatullah, P. E. Di Cesare, P. A. Meere, and G. C. Pereira, “Identification of the Landmark Registration Safe Zones During Total Knee Arthroplasty Using

- an Imageless Navigation System,” *Journal of Arthroplasty*, vol. 28, no. 6, 2013, doi: 10.1016/j.arth.2012.12.013.
- [8] B. Schlatterer, J. M. Linares, P. Chabrand, J. M. Sprael, and J. N. Argenson, “Influence of the optical system and anatomic points on computer-assisted total knee arthroplasty,” *Orthopaedics and Traumatology: Surgery and Research*, vol. 100, no. 4, pp. 395–402, 2014, doi: 10.1016/J.OTSR.2013.12.029.
- [9] “Anatomical Terminology | SEER Training.”  
<https://training.seer.cancer.gov/anatomy/body/terminology.html> (accessed Feb. 19, 2023).
- [10] J. Gordon Betts *et al.*, *Anatomy and Physiology*. Houston, Texas: OpenStax, 2013.
- [11] J. A. McGeough, *The Engineering of Human Joint Replacements*. John Wiley & Sons, 2013. doi: 10.1002/9781118536834.
- [12] V. B. Duthon, C. Barea, S. Abrassart, J. H. Fasel, D. Fritschy, and J. Ménétrey, “Anatomy of the anterior cruciate ligament,” *Knee Surgery, Sports Traumatology, Arthroscopy*, vol. 14, no. 3, pp. 204–213, 2006, doi: 10.1007/s00167-005-0679-9.
- [13] “Ligament Injuries to the Knee | Johns Hopkins Medicine.”  
<https://www.hopkinsmedicine.org/health/conditions-and-diseases/ligament-injuries-to-the-knee> (accessed Feb. 19, 2023).
- [14] J. R. Witstein, “Collateral Ligament Injuries,” *OrthoInfo*, Dec. 2021.  
<https://orthoinfo.aaos.org/en/diseases--conditions/collateral-ligament-injuries/> (accessed Mar. 31, 2023).
- [15] J. B. S. N. Nogueira, L. H. Do Carmo Araujo, and M. J. C. Bezerra, “Planning Primary Total Knee Arthroplasties,” in *Primary Total Knee Arthroplasty*, London: IntechOpen, 2018. Accessed: Jan. 01, 2023. [Online]. Available: <https://www.intechopen.com/chapters/58841>



- [16] C. Batailler, D. Hannouche, F. Benazzo, and S. Parratte, “Concepts and techniques of a new robotically assisted technique for total knee arthroplasty: the ROSA knee system,” *Archives of Orthopaedic and Trauma Surgery*, vol. 141, no. 12, pp. 2049–2058, 2021, doi: 10.1007/s00402-021-04048-y.
- [17] F. R. Middleton and S. H. Palmer, “How accurate is Whiteside’s line as a reference axis in total knee arthroplasty?,” *Knee*, vol. 14, no. 3, pp. 204–207, 2007, doi: 10.1016/j.knee.2007.02.002.
- [18] M. ; Park *et al.*, “Modified Whiteside’s Line-Based Transepicondylar Axis for Imageless Total Knee Arthroplasty,” *Mathematics*, vol. 10, no. 19, p. 3670, Oct. 2022, doi: 10.3390/MATH10193670.
- [19] W. P. Yau, K. Y. Chiu, and W. M. Tang, “How Precise is the Determination of Rotational Alignment of the Femoral Prosthesis in Total Knee Arthroplasty. An In Vivo Study,” *Journal of Arthroplasty*, vol. 22, no. 7, pp. 1042–1048, Oct. 2007, doi: 10.1016/J.ARTH.2006.12.043.
- [20] E. Beretta, E. de Momi, V. Camomilla, A. Cereatti, A. Cappozzo, and G. Ferrigno, “Hip joint centre position estimation using a dual unscented Kalman filter for computer-assisted orthopaedic surgery,” *J Engineering in Medicine*, vol. 228, no. 9, 2014, doi: 10.1177/0954411914551854.
- [21] A. S. Shahi *et al.*, “Special Considerations in Asian Knee Arthroplasty,” *Arthroplasty - Update*, Feb. 2013, doi: 10.5772/53595.
- [22] S. Tsukada, H. Ogawa, M. Nishino, K. Kurosaka, and N. Hirasawa, “Augmented reality-based navigation system applied to tibial bone resection in total knee arthroplasty,” *Journal of Experimental Orthopaedics*, vol. 6, no. 1, pp. 1–7, Dec. 2019, doi: 10.1186/S40634-019-0212-6/TABLES/1.
- [23] D. O. Kendoff, A. Moreau-Gaudry, C. Plaskos, C. Granchi, T. P. Sculco, and A. D. Pearle, “A Navigated 8-in-1 Femoral Cutting Guide for Total Knee Arthroplasty.

- Technical Development and Cadaveric Evaluation,” *Journal of Arthroplasty*, vol. 25, no. 1, pp. 138–145, Jan. 2010, doi: 10.1016/j.arth.2008.11.006.
- [24] S. Pande and P. Dhattrak, “Recent developments and advancements in knee implants materials, manufacturing: A review,” *Materials Today: Proceedings*, vol. 46, pp. 756–762, 2021, doi: 10.1016/J.MATPR.2020.12.465.
- [25] B. C. Carr and T. Goswami, “Knee implants – Review of models and biomechanics,” *Materials & Design*, vol. 30, no. 2, pp. 398–413, Feb. 2009, doi: 10.1016/J.MATDES.2008.03.032.
- [26] D. W. Liu, S. Martinez Martos, Y. Dai, and E. M. Beller, “The femoral intercondylar notch is an accurate landmark for the resection depth of the distal femur in total knee arthroplasty,” *Knee Surgery & Related Research*, vol. 34, no. 1, pp. 1–7, 2022, doi: 10.1186/s43019-022-00159-x.
- [27] T. B. Rodrigues, C. Ó Catháin, N. E. O’Connor, and N. Murray, “A Quality of Experience assessment of haptic and augmented reality feedback modalities in a gait analysis system,” *PLoS One*, vol. 15, no. 3, p. e0230570, 2020, doi: 10.1371/JOURNAL.PONE.0230570.
- [28] M. T. Ae *et al.*, “Computer-assisted total knee arthroplasty versus the conventional technique: how precise is navigation in clinical routine?”, doi: 10.1007/s00167-007-0399-4.
- [29] E.-K. Song *et al.*, “Robotic-assisted TKA Reduces Postoperative Alignment Outliers and Improves Gap Balance Compared to Conventional TKA Clinical Orthopaedics and Related Research ®,” *Clin Orthopaedics & Related Research*, vol. 471, pp. 118–126, 2013, doi: 10.1007/s11999-012-2407-3.
- [30] G. Matziolis, D. Krockner, U. Weiss, S. Tohtz, and C. Perka, “A prospective, randomized study of computer-assisted and conventional total knee arthroplasty: Three-dimensional evaluation of implant alignment and rotation,” *Journal of Bone and Joint Surgery*, vol. 89, no. 2, pp. 236–243, 2007, doi: 10.2106/JBJS.F.00386.

- [31] R. A. Siston, N. J. Giori, S. B. Goodman, and S. L. Delp, "Surgical navigation for total knee arthroplasty: A perspective," *Journal of Biomechanics*, vol. 40, no. 4, pp. 728–735, 2007, doi: 10.1016/j.jbiomech.2007.01.006.
- [32] Y. S. Brin, I. Livshetz, J. Antoniou, S. Greenberg-Dotan, and D. J. Zukor, "Precise landmarking in computer assisted total knee arthroplasty is critical to final alignment," *Journal of Orthopaedic Research*, vol. 28, no. 10, pp. 1355–1359, Oct. 2010, doi: 10.1002/JOR.21139.
- [33] A. Siddiqi, W. M. Hardaker, K. K. Eachempati, and N. P. Sheth, "Advances in computer-aided technology for total knee arthroplasty," *Orthopedics*, vol. 40, no. 6, pp. 338–352, 2017, doi: 10.3928/01477447-20170831-02.
- [34] R. Schwarzkopf, M. Meftah, S. E. Marwin, M. A. Zabat, J. M. Muir, and I. R. Lamb, "The use of imageless navigation to quantify cutting error in total knee arthroplasty," *Knee Surgery & Related Research*, vol. 33, no. 1, pp. 1–9, Dec. 2021, doi: 10.1186/S43019-021-00125-Z/FIGURES/4.
- [35] S. M. Shah, "After 25 years of computer-navigated total knee arthroplasty, where do we stand today?," *Arthroplasty*, vol. 3, no. 1, pp. 1–8, Dec. 2021, doi: 10.1186/S42836-021-00100-9/FIGURES/4.
- [36] E. T. Davis, J. Pagkalos, P. A. M. Gallie, K. Macgroarty, J. P. Waddell, and E. H. Schemitsch, "Defining the Errors in the Registration Process During Imageless Computer Navigation in Total Knee Arthroplasty: A Cadaveric Study," *Journal of Arthroplasty*, 2014, doi: 10.1016/j.arth.2013.06.034.
- [37] W. P. Yau, A. Leung, K. Y. Chiu, W. M. Tang, and T. P. Ng, "Intraobserver Errors in Obtaining Visually Selected Anatomic Landmarks During Registration Process in Nonimage-based Navigation-assisted Total Knee Arthroplasty: A Cadaveric Experiment," *Journal of Arthroplasty*, vol. 20, no. 5, pp. 591–601, Aug. 2005, doi: 10.1016/J.ARTH.2005.02.011.

- [38] B. Schlatterer, J. M. Linares, P. Chabrand, J. M. Sprael, and J. N. Argenson, “Influence of the optical system and anatomic points on computer-assisted total knee arthroplasty,” *Orthopaedics & Traumatology: Surgery & Research*, vol. 100, no. 4, pp. 395–402, Jun. 2014, doi: 10.1016/J.OTSR.2013.12.029.
- [39] F. Figueroa, E. Wakelin, J. Twiggs, and B. Fritsch, “Comparison between navigated reported position and postoperative computed tomography to evaluate accuracy in a robotic navigation system in total knee arthroplasty,” *Knee*, vol. 26, no. 4, pp. 869–875, Aug. 2019, doi: 10.1016/J.KNEE.2019.05.004.
- [40] R. Schwarzkopf, M. Meftah, S. E. Marwin, M. A. Zabat, J. M. Muir, and I. R. Lamb, “The use of imageless navigation to quantify cutting error in total knee arthroplasty,” *Knee Surgery & Related Research*, vol. 33, no. 1, pp. 1–9, Dec. 2021, doi: 10.1186/S43019-021-00125-Z/FIGURES/4.
- [41] L. A. Carlson-Radvansky and G. D. Logan, “The influence of reference frame selection on spatial template construction,” *Journal of Memory and Language*, vol. 37, no. 3, pp. 411–437, Oct. 1997, doi: 10.1006/JMLA.1997.2519.
- [42] J. Johnson, “Tracking and Kinematics.” Mar. 2022.
- [43] G. R. Scuderi, “Total knee arthroplasty performed with inertial navigation within the surgical field,” *Seminars in Arthroplasty*, vol. 25, no. 3, pp. 179–186, Sep. 2014, doi: 10.1053/J.SART.2014.10.009.
- [44] G. Dardenne, Z. Dib, N. Poirier, H. Letissier, C. Lefèvre, and E. Stindel, “What is the best hip center location method to compute HKA angle in computer-assisted orthopedic surgery? In silico and in vitro comparison of four methods,” *Orthopaedics and Traumatology: Surgery and Research*, vol. 105, no. 1, pp. 55–61, Feb. 2019, doi: 10.1016/J.OTSR.2018.11.011.
- [45] C. J. Gatti, B. R. Hallstrom, and R. E. Hughes, “Surgeon variability in total knee arthroplasty component alignment: a Monte Carlo analysis,” *Computer Methods in*

*Biomechanics and Biomedical Engineering*, vol. 17, no. 15, pp. 1738–1750, 2014, doi: 10.1080/10255842.2013.765948.

- [46] F. Paternostre, P. E. Schwab, and E. Thienpont, “The combined Whiteside’s and posterior condylar line as a reliable reference to describe axial distal femoral anatomy in patient-specific instrument planning,” *Knee Surgery, Sports Traumatology, Arthroscopy*, vol. 22, no. 12, pp. 3054–3059, Nov. 2014, doi: 10.1007/S00167-014-2836-5/TABLES/2.
- [47] S. Herregodts *et al.*, “Accuracy of intraoperative bone registration and stereotactic boundary reconstruction during total knee arthroplasty surgery,” *International Journal of Medical Robotics and Computer Assisted Surgery*, Feb. 2022, doi: 10.1002/RCS.2460.
- [48] L. Q. Zhang, D. Xu, G. Wang, and R. W. Hendrix, “Muscle strength in knee varus and valgus,” *Medicine & Science in Sports & Exercise*, vol. 33, no. 7, pp. 1194–1199, 2001, doi: 10.1097/00005768-200107000-00018.
- [49] E. Stindel, D. Gil, J. Briard, P. Merloz, F. Dubrana, and C. Lefevre, “Detection of the center of the hip joint in computer-assisted surgery: An evaluation study of the Surgetics algorithm,” *Computer Aided Surgery* vol. 10, no. 3, pp. 133–139, Jan. 2010, doi: 10.3109/10929080500229975.
- [50] R. A. Siston and S. L. Delp, “Evaluation of a new algorithm to determine the hip joint center,” *Journal of Biomechanics*, vol. 39, no. 1, pp. 125–130, Jan. 2006, doi: 10.1016/J.JBIOMECH.2004.10.032.
- [51] G. Dardenne, Z. Dib, C. Hamitouche, C. Lefèvre, and E. Stindel, “An optimized Least-Moving-Point algorithm to detect the hip center,” vol. 1, pp. 308–302, 2018, doi: 10.29007/clwq.
- [52] F. Marin, H. Mannel, L. Claes, and L. Diirselen, “Brief Report Accurate Determination of a Joint Rotation Center Based on the Minimal Amplitude Point

- Method,” *Computer Aided Surgery*, vol. 8, pp. 30–34, 2003, Accessed: Mar. 08, 2022. [Online]. Available: [www.ie.ncsu.edu](http://www.ie.ncsu.edu).
- [53] N. Lopomo, L. Sun, S. Zaffagnini, G. Giordano, and M. R. Safran, “Evaluation of formal methods in hip joint center assessment: An in vitro analysis”, *Clinical Biomechanics*, vol. 25, no. 3, 2010 doi: 10.1016/j.clinbiomech.2009.11.008.
- [54] C. F. Jekel, *Obtaining non-linear orthotropic material models for pvc-coated polyester via inverse bubble inflation*. Stellenbosch University, 2016. [Online]. Available: <https://hdl.handle.net/10019.1/98627>
- [55] Y. Sumith, “Fast Geometric Fit Algorithm for Sphere Using Exact Solution,” vol. 13244, no. 10, 2015, [Online]. Available: <http://arxiv.org/abs/1506.02776>
- [56] R. A. Siston, A. C. Daub, N. J. Giori, S. B. Goodman, and S. L. Delp, “Evaluation of methods that locate the center of the ankle for computer-assisted total knee arthroplasty,” *Clin Orthop Relat Res*, vol. 439, pp. 129–135, 2005, doi: 10.1097/01.BLO.0000170873.88306.56.
- [57] D. C. Marchant, D. P. Rimmington, R. W. Crawford, S. L. Whitehouse, and J. McGuire, “An algorithm for locating the center of the ankle joint in knee navigation surgery,” *Computer Aided Surgery*, vol. 10, no. 1, pp. 45–49, Jan. 2005, doi: 10.3109/10929080500230536.
- [58] T. Bajd, M. Mihelj, J. Lenarcic, A. Stanovnik, and M. Munih, *Robotics*, vol. 43. 2010. [Online]. Available: <http://journal.um-surabaya.ac.id/index.php/JKM/article/view/2203>
- [59] M. W. Spong, S. Hutchinson, and M. Vidyasagar, “Rigid Motions,” in *Robot Modeling and Control*, 2nd ed. John Wiley & Sons, 2020, pp. 35–67.
- [60] D. P. Meam and C. A. Belta, “Euclidean metrics for motion generation on SE ( 3 ),” *Departmental Papers (MEAM)*, vol. 216, no. 1, pp. 47–60, 2002.

- [61] R. Brégier, F. Devernay, L. Leyrit, and J. L. Crowley, “Defining the Pose of Any 3D Rigid Object and an Associated Distance,” *International Journal of Computer Vision*, vol. 126, no. 6, pp. 571–596, 2018, doi: 10.1007/s11263-017-1052-4.
- [62] G. S. Chirikjian, “Partial Bi-Invariance of SE(3) Metrics,” in *Journal of Computing and Information Science in Engineering*, American Society of Mechanical Engineers (ASME), Mar. 2015. doi: 10.1115/1.4028941.
- [63] G. S. Chirikjian and S. Zhou, “Metrics on motion and deformation of solid models,” *Journal of Mechanical Design, Transactions of the ASME*, vol. 120, no. 2, pp. 252–261, 1998, doi: 10.1115/1.2826966.
- [64] N. Cressie and C. Hardouin, “A diagonally weighted matrix norm between two covariance matrices,” *Spatial Statistics*, vol. 29, pp. 316–328, Mar. 2019, doi: 10.1016/j.spasta.2019.01.001.
- [65] A. Saltelli, “Sensitivity Analysis for Importance Assessment,” *Risk Analysis*, vol. 22, no. 3, pp. 579–590, Jun. 2002, doi: 10.1111/0272-4332.00040.
- [66] M. Taylor, “What is sensitivity analysis?,” 2009. Accessed: Mar. 24, 2023. [Online]. Available: [www.whatisseries.co.uk](http://www.whatisseries.co.uk)
- [67] D. P. Kroese, T. Brereton, T. Taimre, and Z. I. Botev, “Why the Monte Carlo method is so important today,” *Wiley Interdisciplinary Reviews: Computational Statistics*, vol. 6, no. 6, pp. 386–392, Nov. 2014, doi: 10.1002/WICS.1314.
- [68] D. P. Kroese and R. Y. Rubinstein, “Monte Carlo methods,” *Wiley Interdisciplinary Reviews: Computational Statistics* vol. 4, no. 1, pp. 48–58, Jan. 2012, doi: 10.1002/WICS.194.
- [69] “Random Numbers Within a Sphere,” *MathWorks*.  
<https://www.mathworks.com/help/matlab/math/numbers-placed-randomly-within-volume-of-sphere.html> (accessed Mar. 22, 2023).

- [70] “sph2cart,” *MathWorks*.  
<https://www.mathworks.com/help/matlab/ref/sph2cart.html> (accessed Mar. 22, 2023).
- [71] “Spherical Coordinates,” *MathWorks*.  
<https://www.mathworks.com/help/phased/ug/spherical-coordinates.html> (accessed Mar. 22, 2023).
- [72] H. C. Frey and S. R. Patil, “Identification and review of sensitivity analysis methods,” in *Risk Analysis*, 2002, pp. 553–578. doi: 10.1111/0272-4332.00039.
- [73] A. M. Ferrenberg and R. H. Swendsen, “Optimized Monte Carlo Data Analysis,” *Citation: Computers in Physics*, vol. 3, p. 17, 1989, doi: 10.1063/1.4822862.
- [74] S. Dean and B. Illowsky, “Descriptive Statistics: Histogram,” 2009. Accessed: Mar. 24, 2023. [Online]. Available:  
[http://creativecommons.org/licenses/by/2.0/1"SamplingandData:Introduction"<http://cnx.org/content/m16008/latest/>http://cnx.org/content/m16298/1.11/SourceURL:http://cnx.org/content/col110522/latest/SaylorURL:http://www.saylor.org/courses/ma121/](http://creativecommons.org/licenses/by/2.0/1\)
- [75] “Histogram,” *MathWorks*.  
<https://www.mathworks.com/help/matlab/ref/matlab.graphics.chart.primitive.histogram.html> (accessed Mar. 24, 2023).
- [76] M. R. R. Mojumdar and M. Hossain, “Partial derivatives and jacobian matrix,” *Encyclopedia of Electrical and Electronic Power Engineering*, pp. 610–613, Jan. 2023, doi: 10.1016/B978-0-12-821204-2.00083-0.
- [77] W. Shao *et al.*, “Sensitivity analysis of Jacobian determinant used in treatment planning for lung cancer,” in *Proc. SPIE 10574, Medical Imaging 2018: Image Processing*, Houston, Texas, 2018.
- [78] D. Nolte, C. K. Tsang, K. Y. Zhang, Z. Ding, A. E. Kedgley, and A. M. J. Bull, “Non-linear scaling of a musculoskeletal model of the lower limb using statistical



- shape models,” *Journal of Biomechanics*, vol. 49, no. 14, pp. 3576–3581, Oct. 2016, doi: 10.1016/j.jbiomech.2016.09.005.
- [79] S. S. Gardner, D. Dong, L. E. Peterson, K. J. Park, and J. D. Harris, “Is there a relationship between femoral neck-shaft angle and ischiofemoral impingement in patients with hip pain?,” *Journal of Hip Preservation Surgery*, vol. 7, no. 1, pp. 43–48, Jan. 2020, doi: 10.1093/JHPS/HNAA006.
- [80] Intellijoint Surgical, “Intellijoint KNEE Smart Navigation (No CC),” *Youtube*, Feb. 27, 2020. <https://www.youtube.com/watch?v=dnPoxBxbi2E> (accessed Feb. 15, 2023).
- [81] “NDI Optotrack Certus,” *Tracklab*. <https://tracklab.com.au/products/brands/ndi/ndi-optotrak-certus/> (accessed Feb. 15, 2023).
- [82] “3D Coordinates Line of Fit,” *MATLAB Answers*, 2018. <https://www.mathworks.com/matlabcentral/answers/406619-3d-coordinates-line-of-fit> (accessed Mar. 30, 2023).
- [83] “Best Fit Line with 3d Points,” *StackExchange*, 2021. <https://math.stackexchange.com/questions/1611308/best-fit-line-with-3d-points> (accessed Mar. 30, 2023).
- [84] “Fitting a 3D line to a 3D line point cloud,” *StackExchange*, 2013. <https://math.stackexchange.com/questions/268528/fitting-a-3d-line-to-a-3d-line-point-cloud> (accessed Mar. 30, 2023).
- [85] F. Sun, “affine\_fit(X),” 2016. [https://www.mathworks.com/matlabcentral/fileexchange/60502-affine\\_fit-x](https://www.mathworks.com/matlabcentral/fileexchange/60502-affine_fit-x) (accessed Mar. 30, 2023).
- [86] W. P. Yau, A. Leung, K. G. Liu, C. H. Yan, L. L. S. Wong, and K. Y. Chiu, “Interobserver and Intra-observer Errors in Obtaining Visually Selected Anatomical Landmarks During Registration Process in Non-Image-Based

Navigation-Assisted Total Knee Arthroplasty,” *Journal of Arthroplasty*, vol. 22, no. 8, pp. 1150–1161, Dec. 2007, doi: 10.1016/J.ARTH.2006.10.010.

[87] Zimmer Biomet, “ROSA Knee User Manual & Surgical Technique V1.2.” 2022.

# Appendix A

## Bone reference frame code calculated for sensitivity function

```

syms FCx; syms FCy; syms FCz;
syms HCx; syms HCy; syms HCz;
syms Wx1; syms Wy1; syms Wz1;
syms Wx2; syms Wy2; syms Wz2;

%whitesides line
Wx=Wx2-Wx1;
Wy=Wy2-Wy1;
Wz=Wz2-Wz1;
W=[Wx Wy Wz]/norm([Wx Wy Wz]);
Wx=W(1);
Wy=W(2);
Wz=W(3);

%x axis
xx=HCx-FCx;
xy=HCy-FCy;
xz=HCz-FCz;
x=[xx xy xz]/norm([xx xy xz]);
xx=x(1);
xy=x(2);
xz=x(3);

%z axis
zx=xy*Wz-xz*Wy;
zy=xz*Wx-xx*Wz;
zz=xx*Wy-xy*Wx;
z=[zx zy zz]/norm([zx zy zz]);
zx=z(1);
zy=z(2);
zz=z(3);

%y axis
yx=zy*xz-zz*xy;
yy=zz*xx-zx*xz;
yz=zx*xy-zy*xx;
y=[yx yy yz]/norm([yx yy yz]);
yx=y(1);
yy=y(2);
yz=y(3);

%translation vector
Tx=FCx;
Ty=FCy;
Tz=FCz;

```

# Appendix B

## Additional Experimental Result Tables

**Table B.1 Hip center calculation method comparison**

		X (mm)	Y (mm)	Z (mm)	Euclidean Distance (mm)
SB-1	Least Squares	-158.29	-357.88	-1815.04	0.6685
	Geometric	-158.62	-358.46	-1815.08	
SB-2	Least Squares	-170.62	-383.09	-1816.14	1.2680
	Geometric	-171.42	-384.03	-1816.43	
SB-3	Least Squares	-138.50	-203.38	-2253.85	0.0748
	Geometric	-138.46	-203.32	-2253.83	

**Table B.2 Femur landmark errors compared to average**

	Femur Center (mm)	Hip Center (mm)	Whiteside's Line (rad)	Lateral Condyle (mm)	Medial Condyle (mm)
SB-1	1.1329	17.250	0.0507	5.3255	1.3342
SB-2	0.5147	11.629	0.0626	5.9201	1.8306
SB-3	0.3647	8.020	0.0497	2.8589	1.5322
SB-4	0.7218	2.874	0.0383	10.3550	2.0175
TD-1	0.2798	5.7036	0.0717	1.8355	1.2170
TD-2	1.7449	6.9849	0.0387	1.4784	0.6871
TD-3	0.4978	7.1016	0.0500	0.6571	1.3684
TD-4	1.1659	5.8404	0.0492	1.2431	1.0397
Mean	0.803	8.175	0.0514	3.7092	1.3783

**Table B.3 Tibia landmarks compared to average**

	Tibia Center (mm)	Lateral Malleolus (mm)	Medial Malleolus (mm)	AP axis (rad)	Lateral Plateau (mm)	Medial Plateau (mm)
SB-1	4.3065	1.2513	3.8076	0.0952	3.1403	1.8289
SB-2	1.3736	3.0378	0.4450	0.0818	0.7106	1.1407
SB-3	4.0099	3.3579	2.3210	0.1255	1.2907	1.8515
SB-4	1.5928	3.1750	1.7474	0.0682	1.9015	1.9717
TD-1	3.3027	4.8456	4.8223	0.2008	7.4657	8.9443
TD-2	3.0709	2.6977	6.0969	0.1686	8.4157	8.2155
TD-3	3.4758	4.8347	2.6788	0.1415	10.5210	5.9965
TD-4	2.6548	7.2003	8.8068	0.2628	5.2990	3.7340
Average	2.973	3.800	3.84	0.143	4.8431	4.2104

**Table B.4 Bone reference frame metric values for 3D printed bone**

Trial and bone	Bone frame metric on SE(3) value
TD-1 Femur	1.114
TD-2 Femur	2.898
TD-3 Femur	0.7408
TD-4 Femur	Ideal
TD-1 Tibia	6.1761
TD-2 Tibia	6.4976
TD-3 Tibia	Ideal
TD-4 Tibia	2.755

**Table B.5 Lateral and Medial Condyle Errors from Ideal Trial along mechanical axis**

	Lateral Condyle (mm)	Medial Condyle (mm)
SB-1	0.1675	0.0823
SB-2	0.2121	0.1913
SB-3	Ideal	Ideal
SB-4	6.1026	0.327
SB-5	0.5686	0.1292
SB-6	0.2518	0.4899

**Table B.6 Lateral and Medial Plateau Errors from Ideal Trial along mechanical axis**

	Lateral Plateau (mm)	Medial Plateau (mm)
SB-1	0.6523	0.706
SB-2	Ideal	Ideal
SB-3	0.5036	0.6309
SB-4	0.6296	1.0389
SB-5	1.0106	2.0269
SB-6	1.0265	3.2824



## Curriculum Vitae

**Name:** Nicole Martensson

**Post-secondary Education and Degrees:** Western University  
London, Ontario, Canada  
2017-2021 B.E.Sc. Mechatronic Systems Engineering

Western University  
London, Ontario, Canada  
2021-2023 M.E.Sc. Electrical and Computer Engineering

**Honours and Awards:** Professional Engineers Ontario London Scholarship  
2017

Natural Science and Engineering Research Council (NSERC)  
Canada Graduate Scholarship-Masters  
2021-2022

Ontario Graduate Scholarship  
2022-2023

**Related Work Experience** Teaching Assistant  
The University of Western Ontario  
2021-2023

### Presentations:

The Effect of Landmark Acquisition Errors During Computer-Navigated Knee Surgery  
Using a Simulated Model

*Winning Presentation in the Robotics and Controls Category of the 2022 Electrical and Computer Engineering Graduate Research Symposium, Western University*

### Publications:

J. Kusins, N. Knowles, N. Martensson, M. P Columbus, G. S. Athwal, and L. M Ferreira,  
“Full-field experimental analysis of the influence of microstructural parameters on the  
mechanical properties of humeral head trabecular bone,” *Journal of orthopaedic research*,  
2021, doi: 10.1002/jor.25242.